Fermi National Accelerator Laboratory
P.O. Box 500 - Batavia, Illinois - 60510

Fermilab Engineering Document
1MW NUMI AIP HORN 1 AIR DIVERTER TEST STUDY
ED0009631, Rev. -

Rev.	Date	Description	Originated By	Checked By	Approved By
-	22 JAN 2013	Initial Release	*Cory Crowley, Ang Lee, George Lolov, Lionel Pittman, & Zhijing Tang*		

Table of Contents

I.	Introduction	3
II.	Existing Diverter Design	4
	1. Specifications	4
	2. Known Cooling Coefficients on Stripline	5
III.	Stripline Analysis Findings at 1MW	6
	1. Boundary Conditions	6
	2. Steady State Temperature	6
	3. Steady State Stress	7
	4. Transient Stress	9
	5. Initial Conclusions	11
IV.	CFD Studies	11
	1. Modeling Efforts	11
	2. Pressure Measurements	12
V.	Revised Diverter Design	14
	1. Overview	14
	2. Specifications	18
VI.	Supplemental T-Block Diverter	19
	1. Initial Concept	19
	2. Pursued Design	20
	3. Diverter Angle Iterations	22
	4. Final Model	24
VII.	Experimental Convection Coefficient Data	25
	1. Test Setup	25
	2. Data	26
	3. Inner Stripline Testing	30
VIII.	Updated 1MW Stripline Analysis	33
	1. Steady State Temperature	33
	2. Transient Temperature	34
	3. Deformation	35
	4. Transient Stress	35
IX.	Conclusion	36

I. Introduction

The 1MW NuMI Accelerator Improvement Project (AIP) is a wide-ranging upgrade project to the NuMI target hall facility, focusing on facility systems, beamline components, and instrumentation. A critical beamline element, Horn 1, which has been most recently redesigned for reliable 700kW operation, will be a limiting factor with regards to acceptance of beam energy deposition on its current supply bus structure. This structure is internally referred to as the stripline, shown in figure 1.1, and represents one of two subassemblies of concern on Horn 1 at 1MW operation. The second structure is the horn inner conductor, as it sees the majority of beam spray / pion interaction, but this structure has been analyzed and documented separately in ED0007371 and found to be adequate given additional interior water cooling.

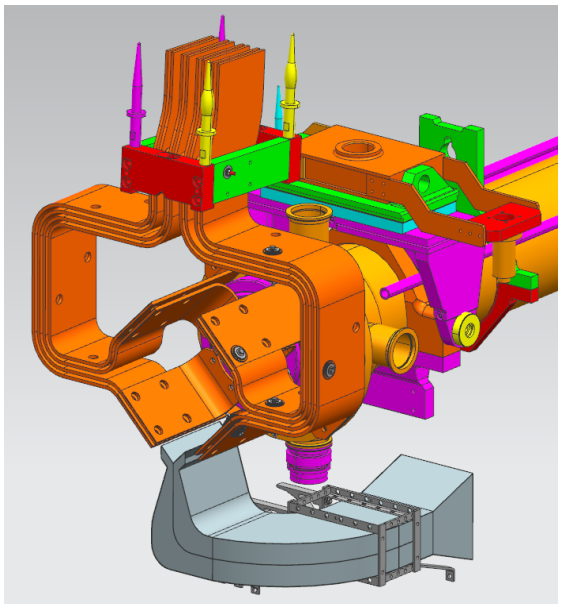

Figure 1.1 NuMI 700kW stripline & air diverter.

The revised beam parameters for 1MW operation can be seen below in table 1.1 and will feed into the cumulative EDEP & joule heating loads that the stripline structure must withstand.

Proton Beam Energy (GeV)	Protons / Cycle	Cycle Time (sec)	Beam Power (MW)	Horn Current (kA)	Current Pulse Width (ms)
120	6.5E+13	1.2	1.0	200	2.3

Table 1.1 1MW NuMI AIP beam & pulse parameters.

It is known from prior analysis efforts that the stripline structure has an operating temperature on the order of 100C during 700kW operation, and that essentially represents the highest allowable operating temperature for any stressed aluminum structure in NuMI / NOvA beamline operations. Therefore, for successful 1MW operation which also meets the TSD threshold of 100,000,000 pulse life, additional cooling advancements are required. This document entails operation of the stripline at 1MW without any additional cooling, the additional cooling studies performed, design directions taken, and finally, the resultant operating temperatures of the stripline with planned cooling upgrades. The analysis & designs below will show that <100C is possible at 1MW operation while also maintaining acceptable fatigue life for 100,000,000 pulses.

II. Existing Diverter Design

1. Specifications

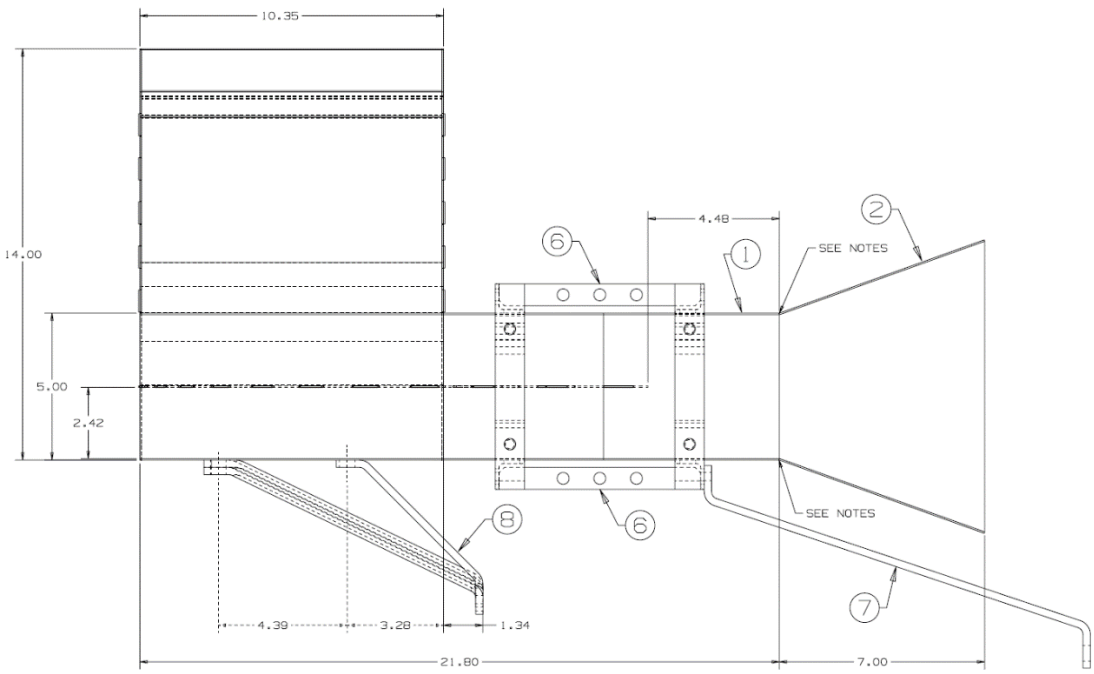

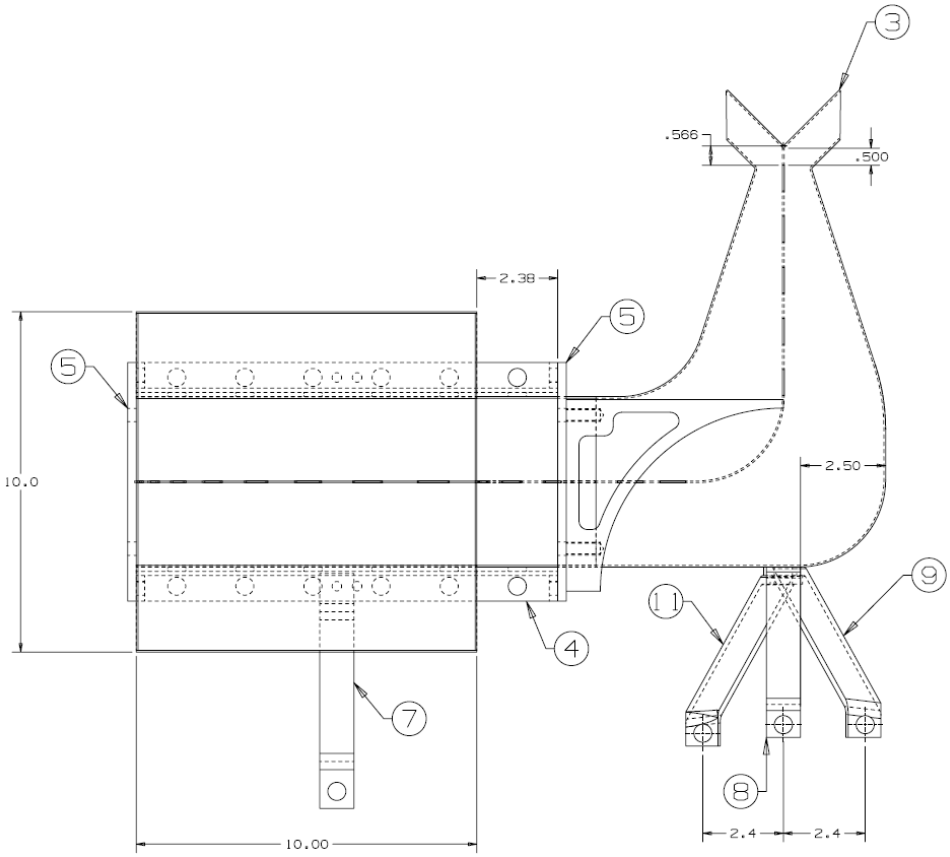

Figures 2.1.1 & 2.1.2 Existing stripline air diverter design.

2. Known Cooling Coefficients on Stripline

Previous wind tunnel studies have shown that the addition of an air diverter, as opposed to the original NuMI horn with no ducted cooling, makes a substantial impact on heat transfer coefficients. It was a result of 700kW operation with an older style stripline that demanded this change. Furthermore, as a baseline analysis for comparison of current 700kW operation vs. anticipated 1MW operation, the below convection coefficients were used according to the position described in figure 2.2.1.

Segment #	External (W/m2·K)	Internal (W/m2·K)
1	5	2
2	15	5
3	36	5
4	36	5
5	36	5
6	36	5
7	36	5
8	15	5

Table 2.2.1 Original convection coefficients (segments 1-8).

	Outer Flag		Inner Flag	
	External	internal	External	internal
9	28	5	18	5
10	10	5	10	5
11	10	NA	10	NA

Table 2.2.2 Original convection coefficients (segments 9-11).

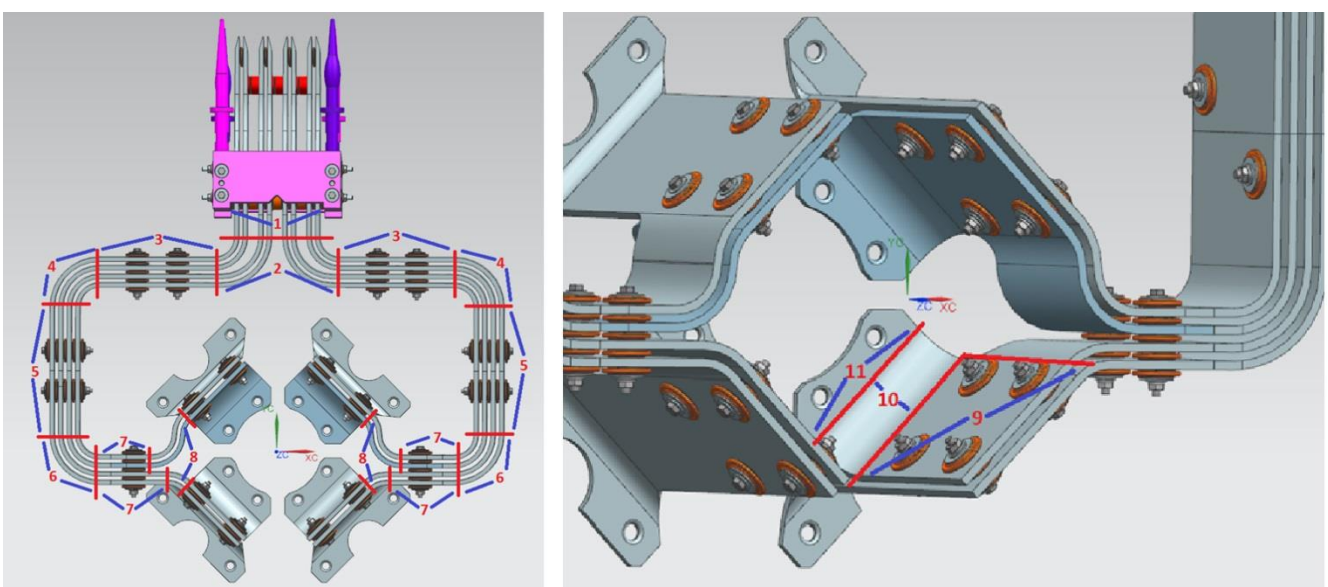

Figure 2.2.1 Stripline convection coefficient regions.

III. Stripline Analysis Findings at 1MW

1. Boundary Conditions

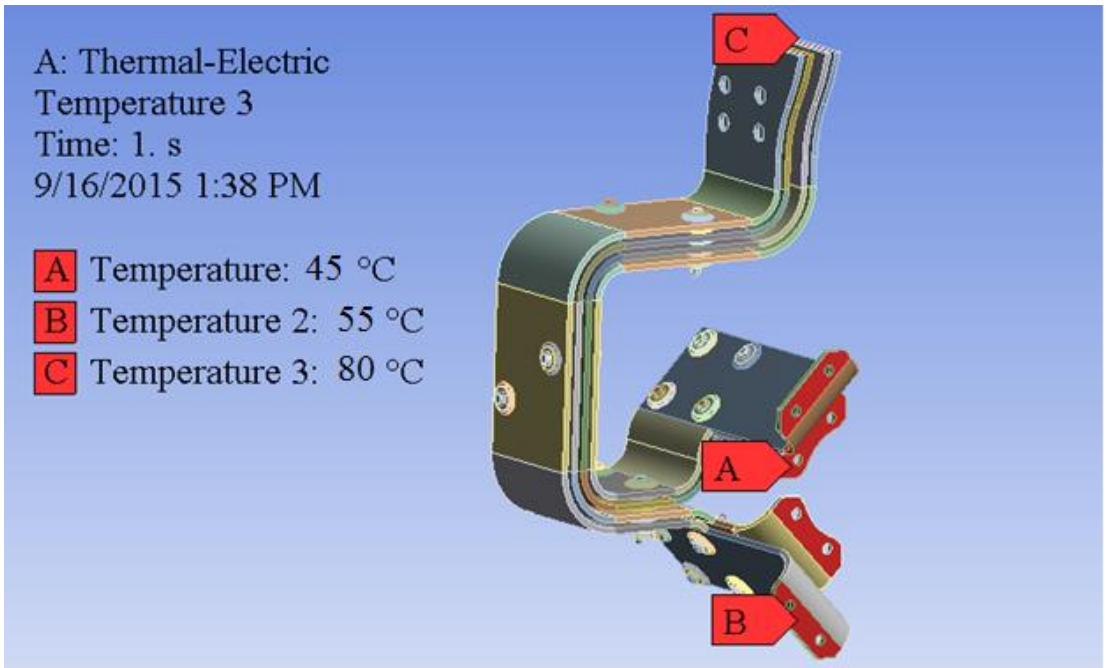

Figure 3.1.1 Boundary conditions of unmodified stripline at 1MW operation.

2. Steady State Temperature

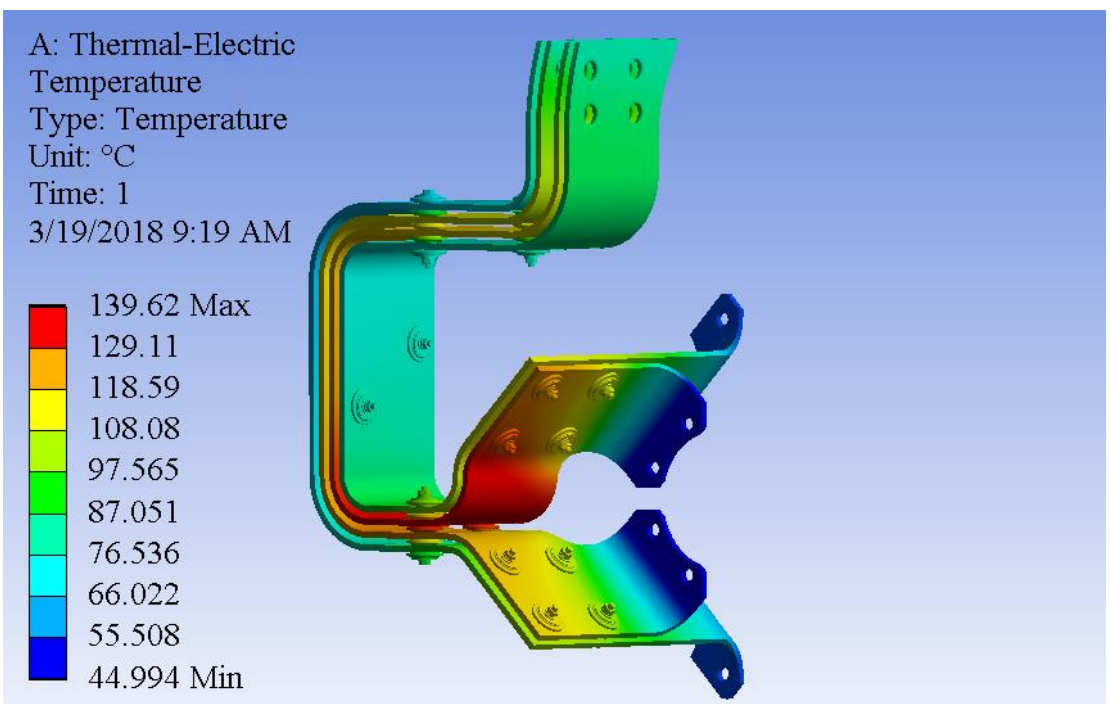

Figure 3.1.2 Steady state temperature of unmodified stripline at 1MW operation.

3. Steady State Stress

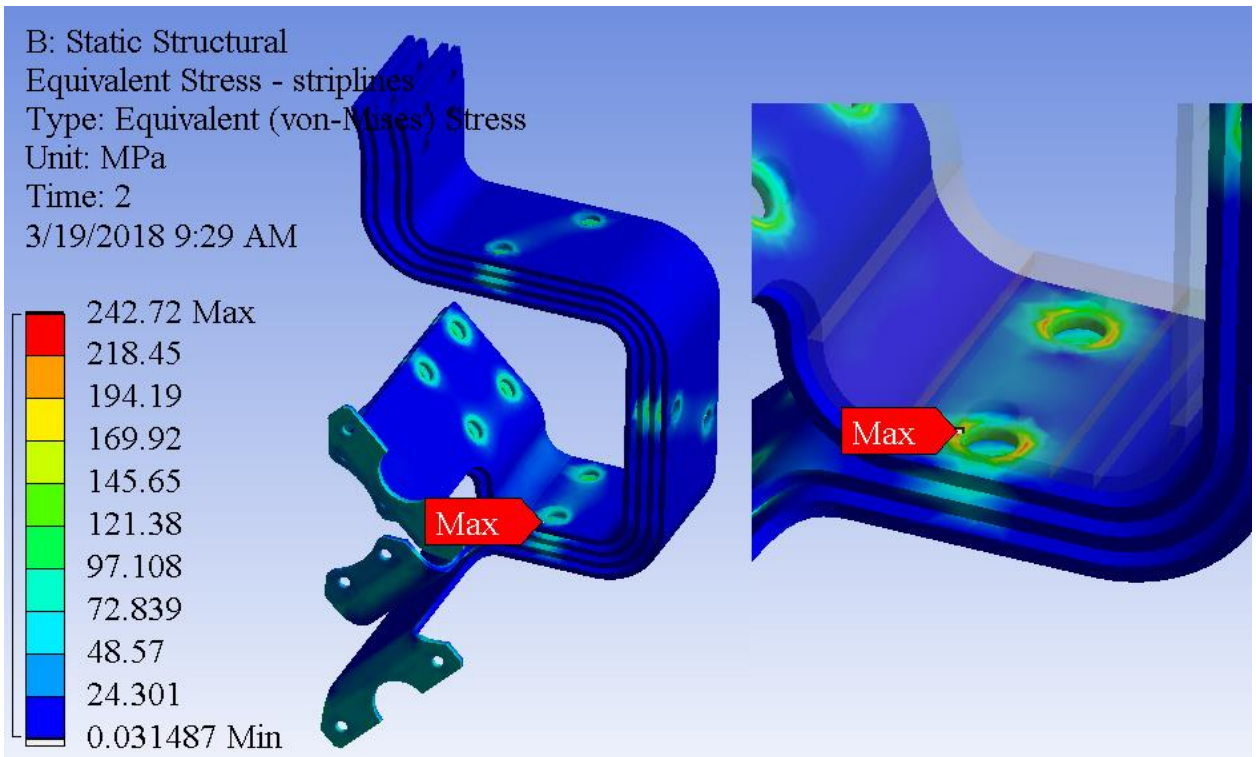

Figure 3.3.1 Steady state stress of unmodified stripline at 1MW operation.

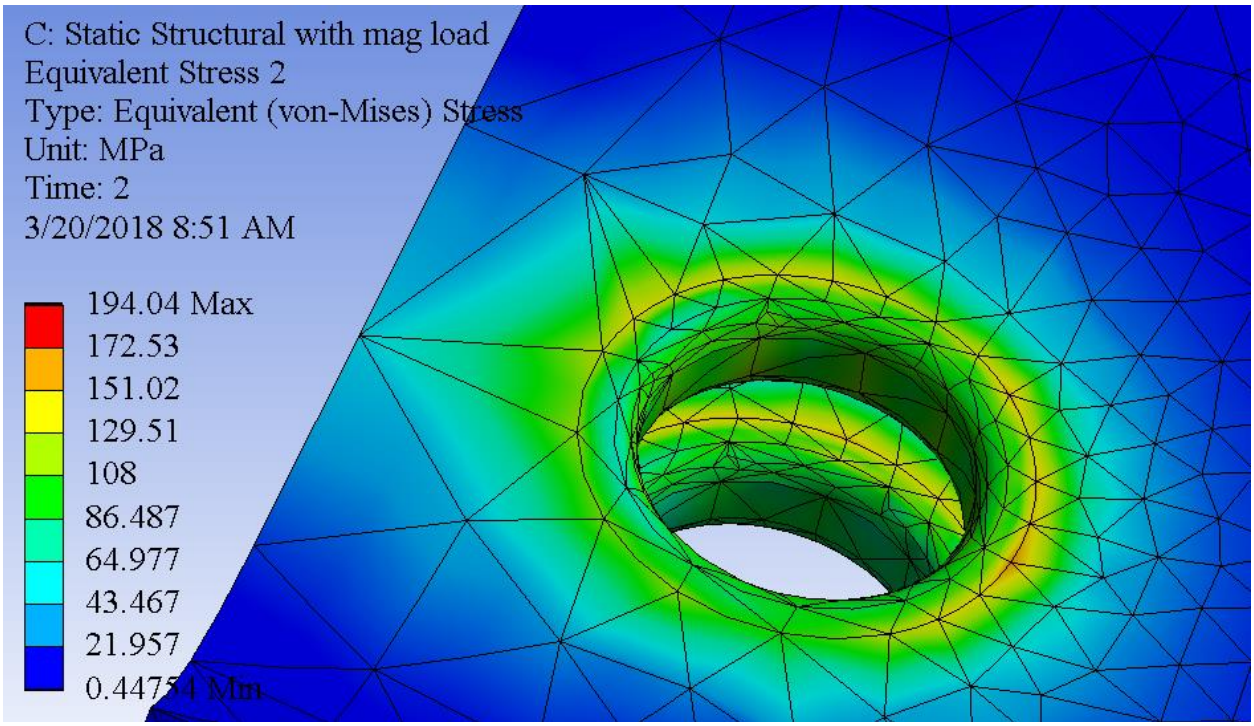

Figure 3.3.2 Steady state stress of unmodified stripline at 1MW operation

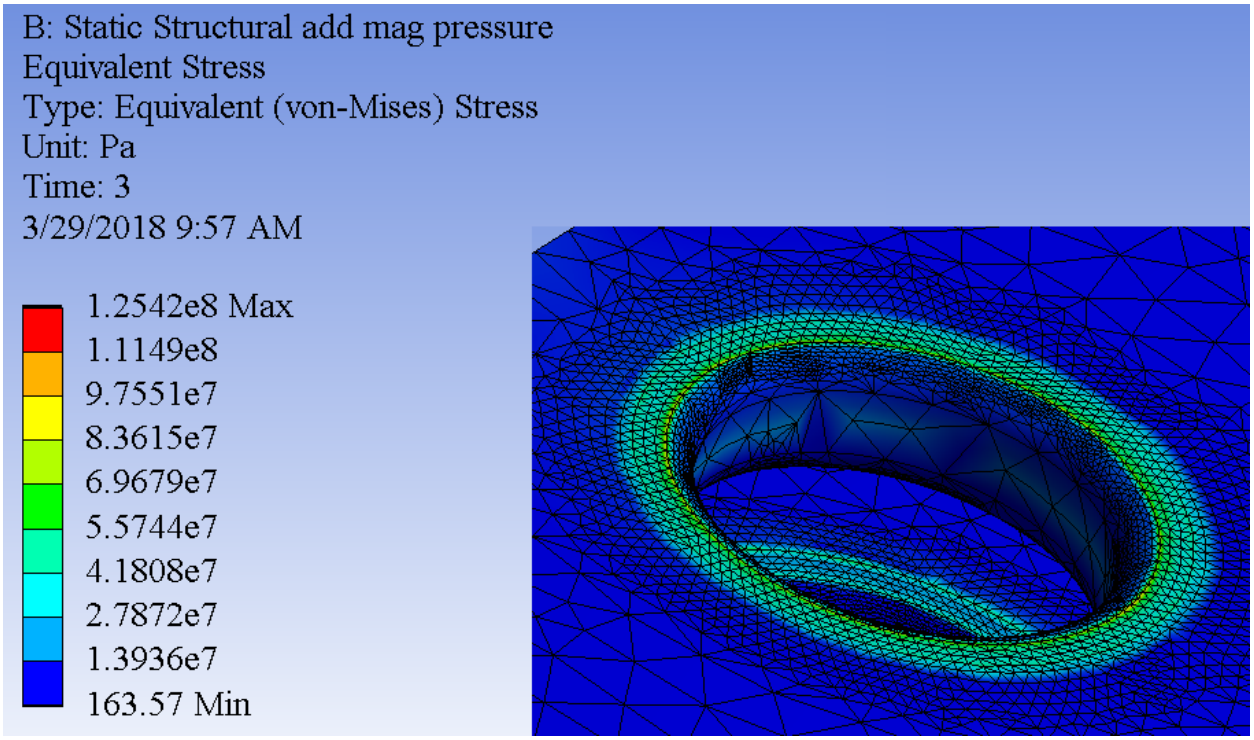

Figure 3.3.3 Steady state stress of unmodified stripline at 1MW operation.

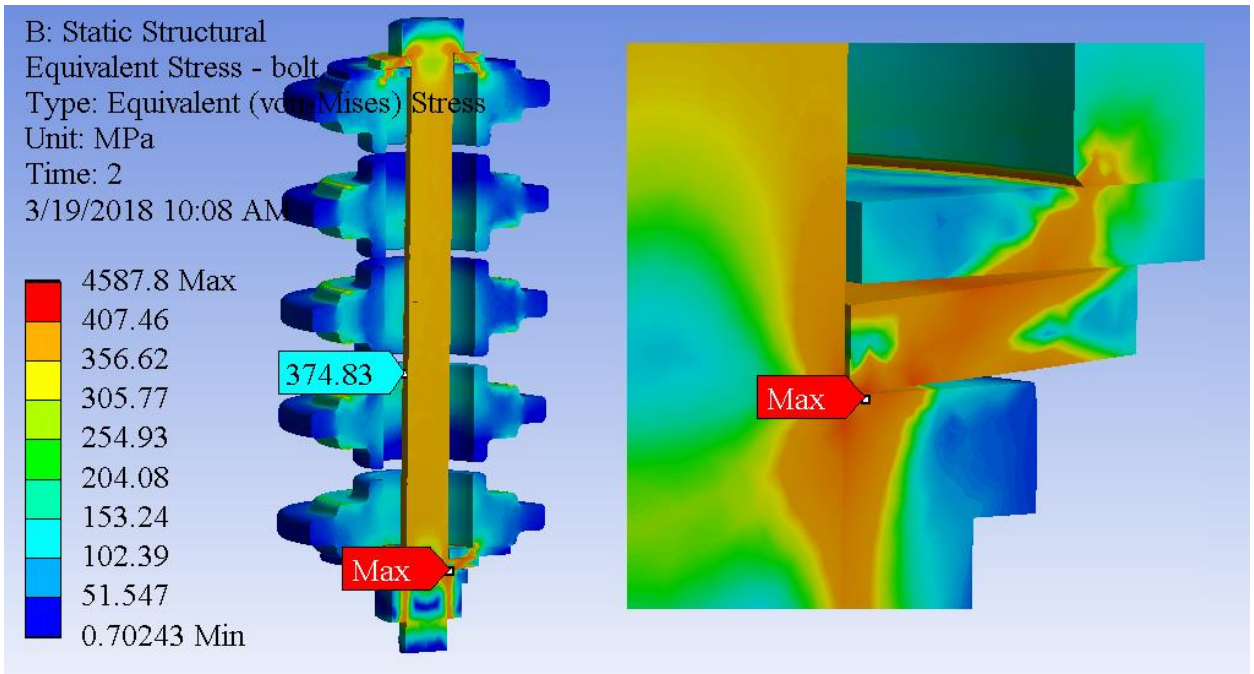

Figure 3.3.4 Steady state stress of unmodified stripline at 1MW operation.

4. Transient Stress

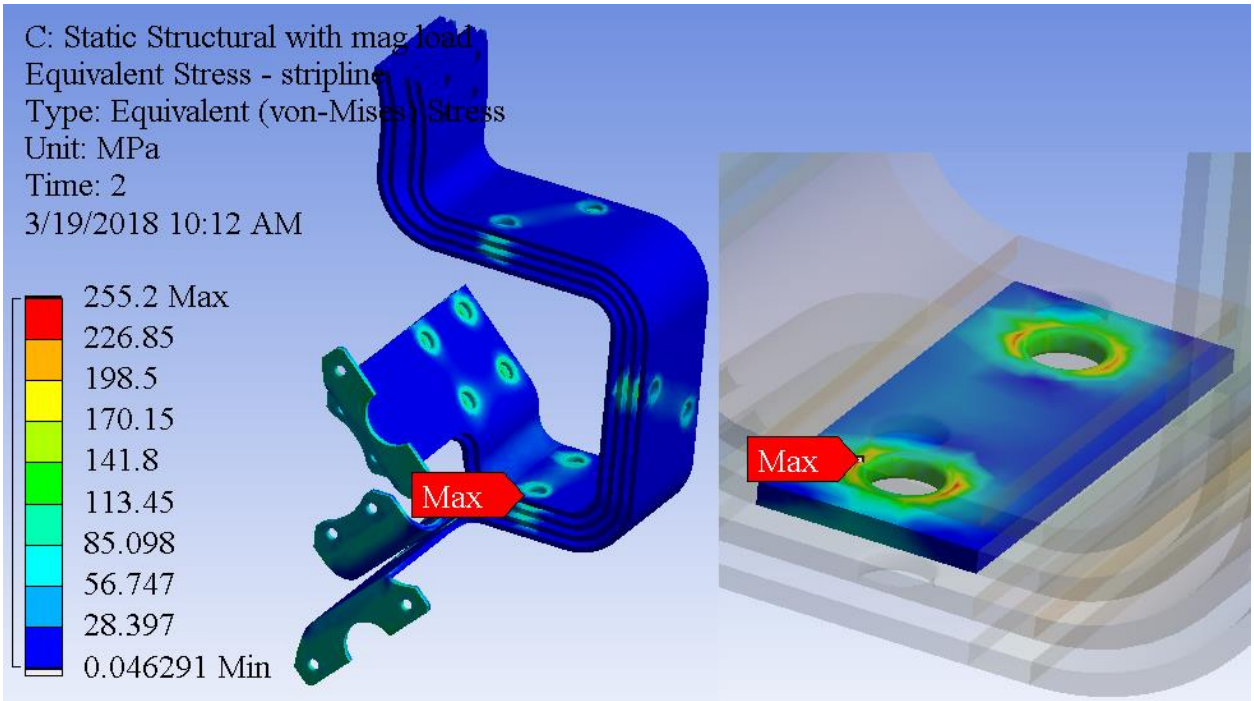

Figure 3.4.1 Transient stress of unmodified stripline at 1MW operation.

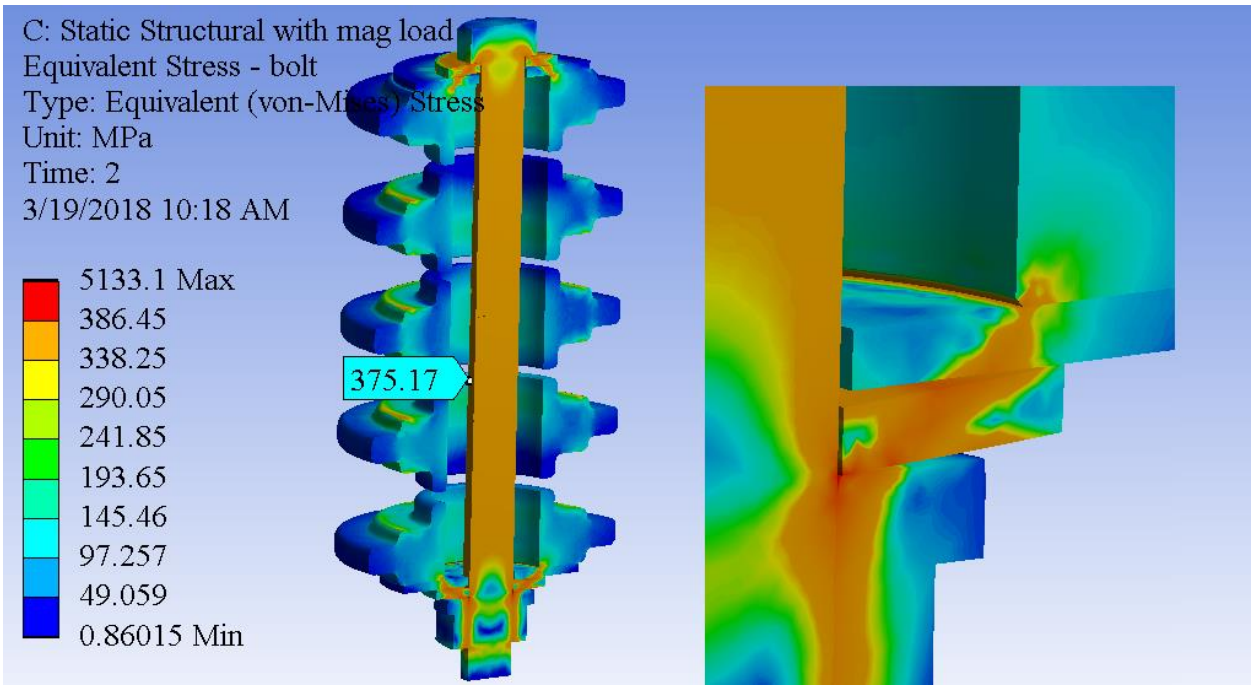

Figure 3.4.2 Transient stress of unmodified stripline at 1MW operation.

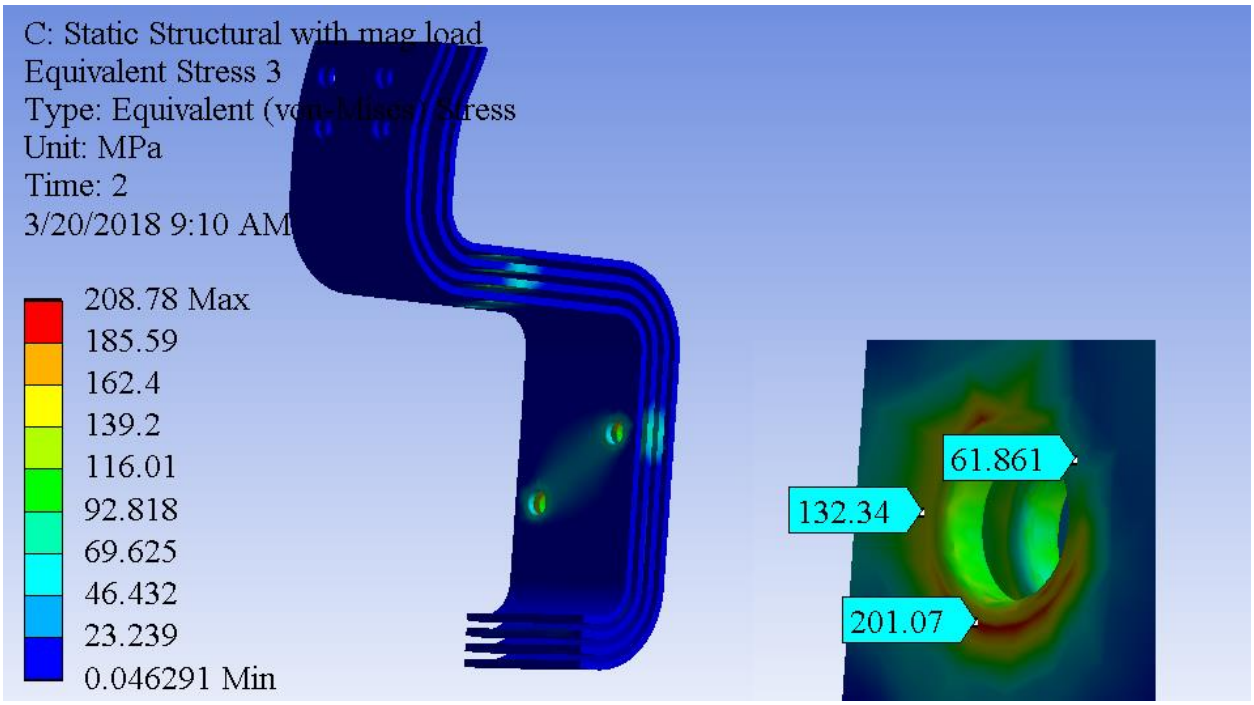

Figure 3.4.3 Transient stress of unmodified stripline at 1MW operation.

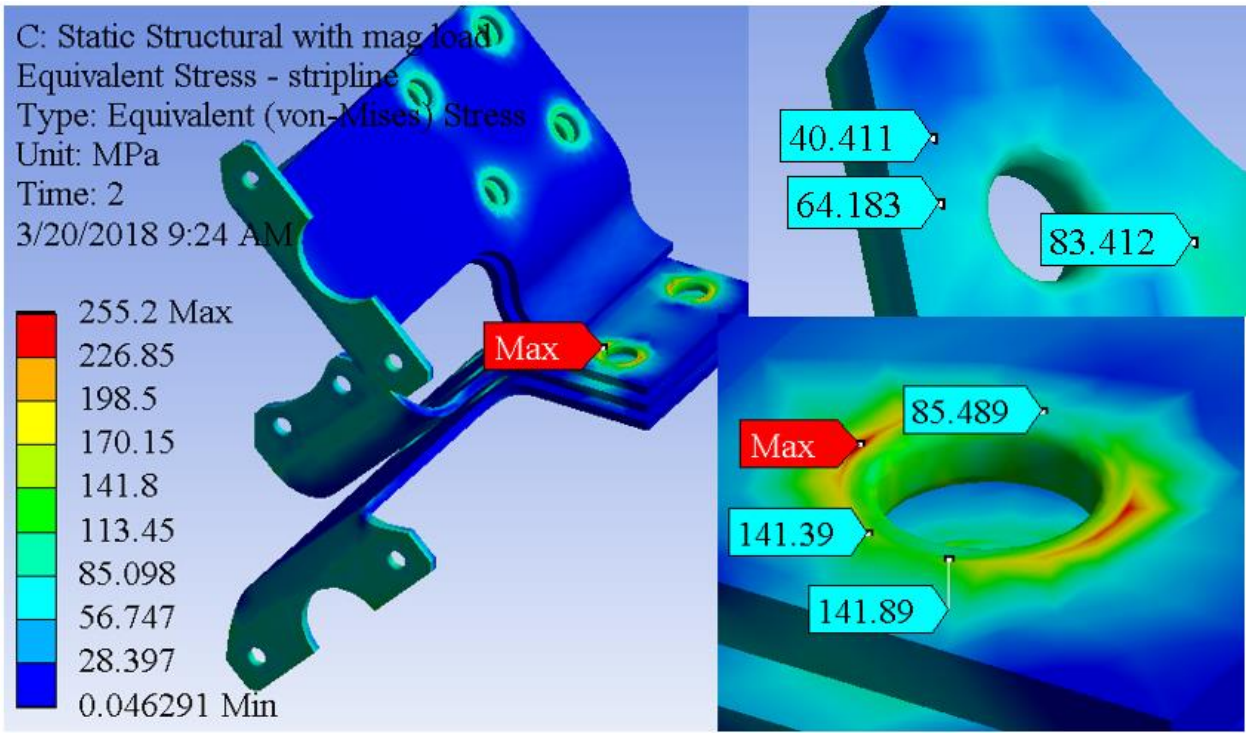

Figure 3.4.4 Transient stress of unmodified stripline at 1MW operation.

		Stress (MPa)			Stress ratio		Fatigue Safety Factor (10^8)
Material	Position	Smax	Sm	Sa	Su/Smax	Sy/Smax	
6101	Bolt hole	132	124	8	1.5	1.3	1.3
6013	Bolt hole	141	135	6	2.2	2.0	2.0
6013	connection	65	57	8	4.7	4.4	4.0

Table 3.4.1 Unmodified stripline stresses at 1MW.

5. Initial Conclusions

1) The higher strength 6013-T6 material will help prevent failure of the strip line.
2) Since the alternate stress is quite small compared with mean stress, mean stress dominates in Goodman equation used to calculate the fatigue safety factor. The mean stress is caused by bolt pretension & this kind of stress is a secondary stress because it is caused by the displacement. As time goes on, the stress will lessen. Therefore, actual fatigue safety factor may increase over time.
3) The overall stripline temperature is too high as it is under present cooling conditions. An improvement is needed in cooling efficiency.

IV. CFD Studies

1. Modeling Efforts

The initial CFD setup contains the NUMI horn geometry placed in a box that represented the lower chase dimensions. A solid/fluid mesh was created using OPENFoam Hex Meshing scheme, which produced a mesh of 3.5*10^6 elements. The working fluid was room temperature air with volumetric flow rates of 25000 cfm and 10000 cfm for comparative purposes. The images show the streamlines that pass thru the air diverter, and furthermore the CFD shows that NUMI horn geometry acts as blockage relative to the flags and produces a stagnation zone of fluid. This stagnation zone would produce a poor zone of convective heat transfer in this region. This simulation was done in an isothermal scheme and the horn geometry acted as a boundary wall.

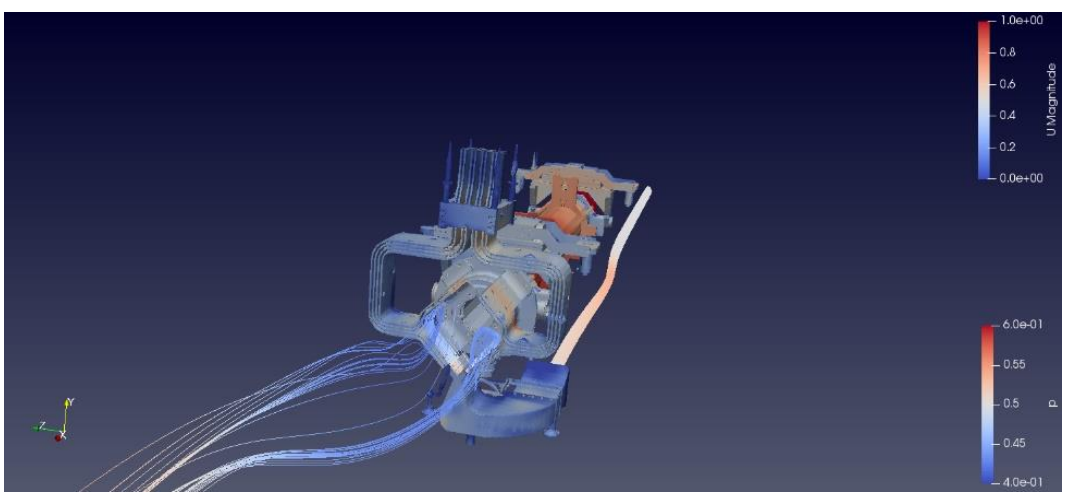

Figure 4.1.1 Existing Horn 1 CFD run assuming 25,000 CFM chase air flow & current diverter.

Figure 4.1.1 shows the streamline of the diverted air, which is only coming into contact with the bottom flags of the strip line before it flows to the outlet of the chase. A metric of interest was the fluid velocities above the inner flag surfaces. While the bottom flags on average had fluid velocity of 3 m/s to 3.46 m/s the top flags had average fluid velocity of .5 m/s to .72 m/s. This low fluid velocity near the surface of the top flags would relate to low heat convection occurring in that region. Multiple air diverter designs were used in the CFD study, and although diverters with larger cross-sectional inlets produced greater flow velocities near the surface of the bottom flag, the diverter flow still minimally interacted with the top inner flags of the horn.

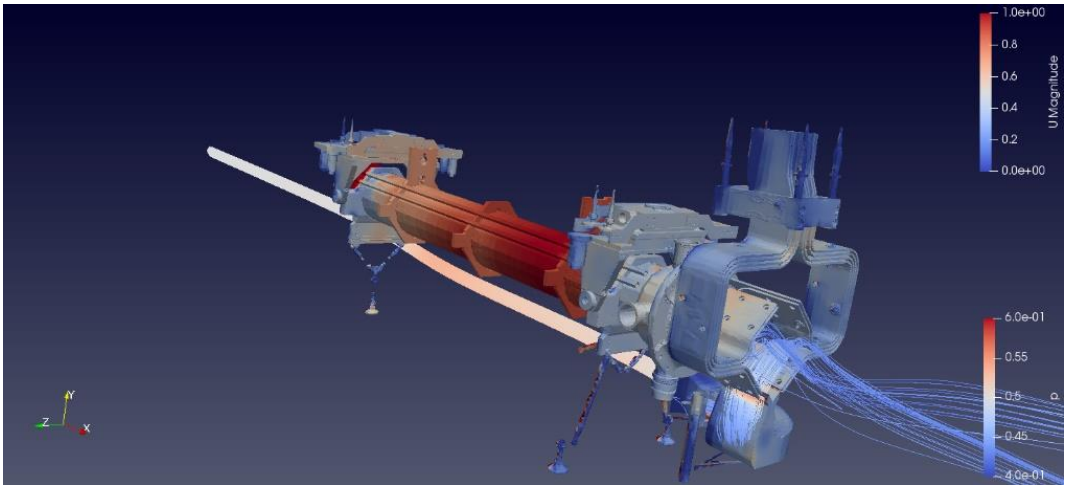

Figure 4.1.2 Revised Horn 1 CFD run with revised diverter.

2. Pressure Measurements

To quickly measure the convection coefficient around the flags for comparative testing, several experimental studies were completed. All utilized a series of pressure measurements in a 3 X 3 grid, obtained with the use of a National Instruments data acquisition system, which captured the pressure and temperature data in real time. The pressure field of all 8 flag surfaces was measured for both the baseline and increased cross sectional area diverters, and to facilitate expedient testing, a manifold was created to measure the pressure on 9 locations of the flag.

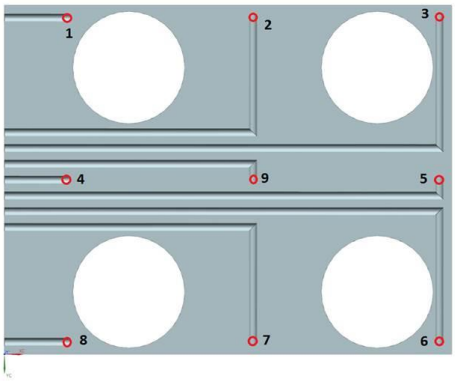

Figure 4.2.1 Pressure manifold port identifiers.

Although flow field results were garnered from this study, the variations in pressure along each flag was negligible. Differences were sufficient to help guide design, but were not usable for convection coefficient calculations. It should be noted however, that there was a noticeable drop in pressure between the baseline and larger diverted testing cases, which is evidence that the flow rate of diverted air increased

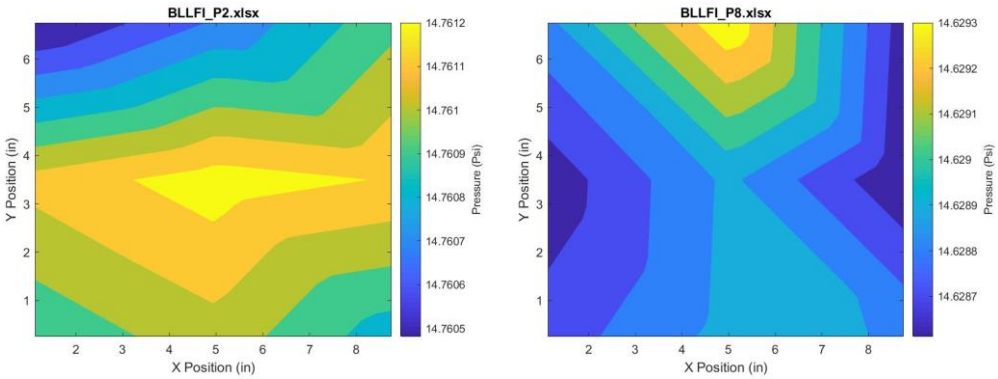

Figure 4.2.2 Pressure flow field measurements (Baseline Diverter (Left), Larger Diverter (right)).

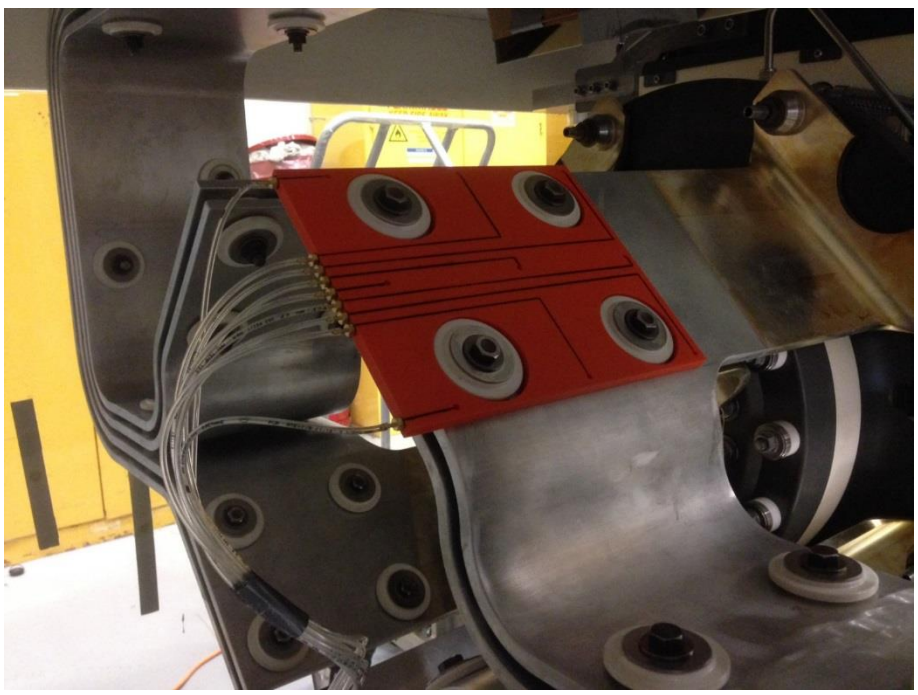

Figure 4.2.3 Pressure manifold placement on flag surface.

V. Revised Diverter Design

1. Overview

In order to increase the amount of airflow to each of the strip line flags and minimize frictional losses in flow, new diverter geometry was created. The original diverter design is shown in figure 5.1.1 and consists of an inlet duct, a middle duct, an outlet duct, and a divider along the center of the ducts that splits up the airflow evenly between each side of the strip line. There are several visible sharp edges around the inlet to middle duct transition and around the outlets that serve as friction hotspots and are detrimental to airflow velocity. In addition, figure 5.1.2 shows that the outlet openings are not symmetrically positioned about the top and bottom lower flags and, as a result, there is little to no airflow across the bottom face of the lower flags.

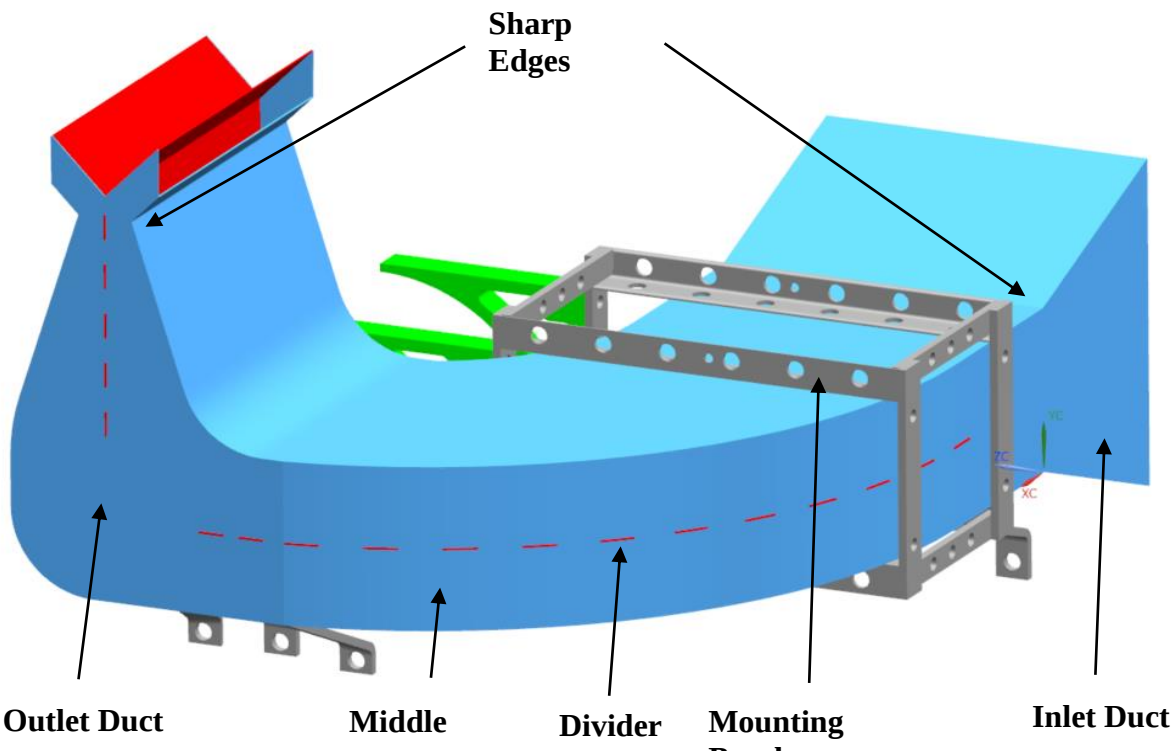

Figure 5.1.1 Original diverter design.

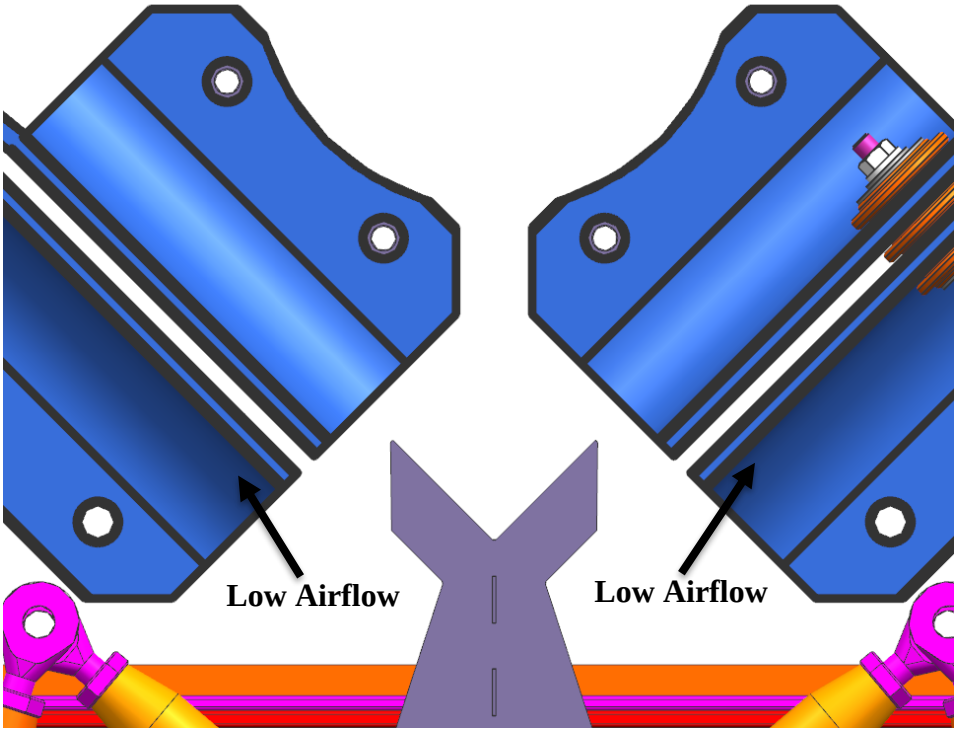

Figure 5.1.2 Original diverter outlet ducts.

The new diverter design, shown in figure 5.1.3, addresses all these issues. Namely, it features updated designs for the inlet and outlet ducts. The two inlet ducts are compared in figure 5.1.4. While the original inlet duct features straight sheets converging to sharp corners around the transition to the middle duct, the new inlet duct features four curved sheets that make the transition smoother. The curvature of the inlet duct was determined by a study that suggests that an elliptical shape is superior for minimizing boundary layer thickness near the duct walls and reducing the length along the duct at which flow becomes fully developed [1]. As such, each of the four sheets were curved into a quarter-ellipse shape with a major axis, *a*, of 9 inches and a minor axis, *b*, of either 1.5, 3, or 5 inches.

The dimensions of the new inlet were chosen such as to maximize the inlet area given the space constraints of surrounding parts and essential horn clearances. The inlet duct depth was maximized to 9 inches to make the major axis of the ellipses as large as possible and thus make the curves as smooth and gradual as possible to aid with flow development. As a result, the inlet area was increased by more than a factor of 2 over the original inlet area, effectively doubling the volumetric flow rate of air traveling through the diverter.

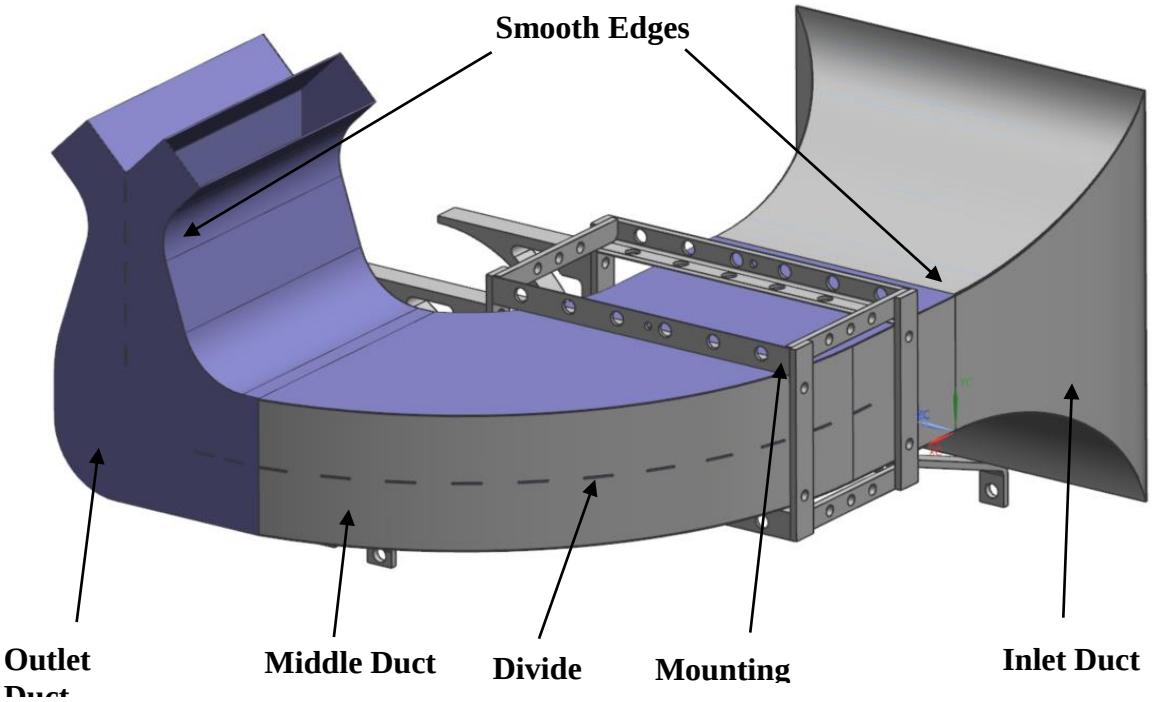

Figure 5.1.3 New diverter design.

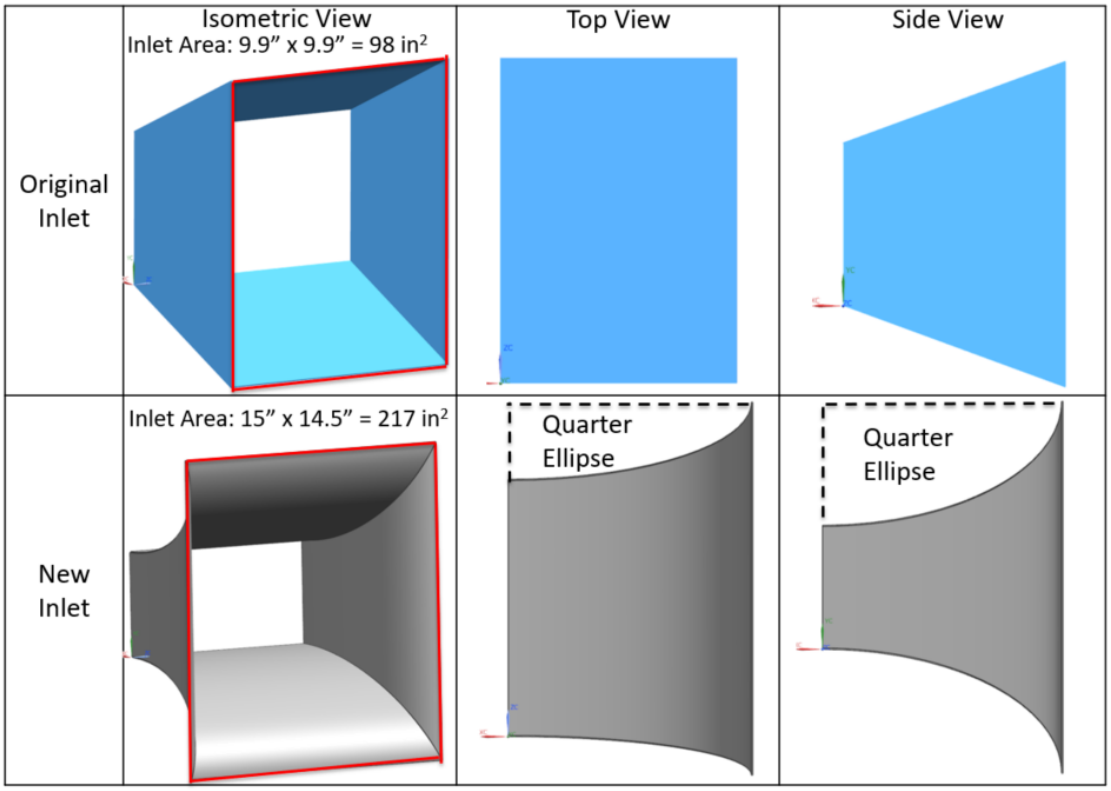

Figure 5.1.4 Original vs. revised inlet duct design.

Because the inlet area was doubled, this allowed for the outlet area to be doubled as well while still maintaining the same volumetric flow rate achieved by the original inlet. However, by increasing the outlet area this allowed the airflow to be more evenly distributed between flag pairs. Figure 5.1.5 shows that airflow could now get to the top, middle, and bottom faces of the lower flags on the strip line. Consequently, this would increase the convection coefficients across the bottom flags and improve cooling. Additionally, it can be seen in figure 5.1.6 that the sharp edges near the exits of the outlet duct were rounded out in an effort to reduce airflow stagnation from frictional effects and the generation of Eddies.

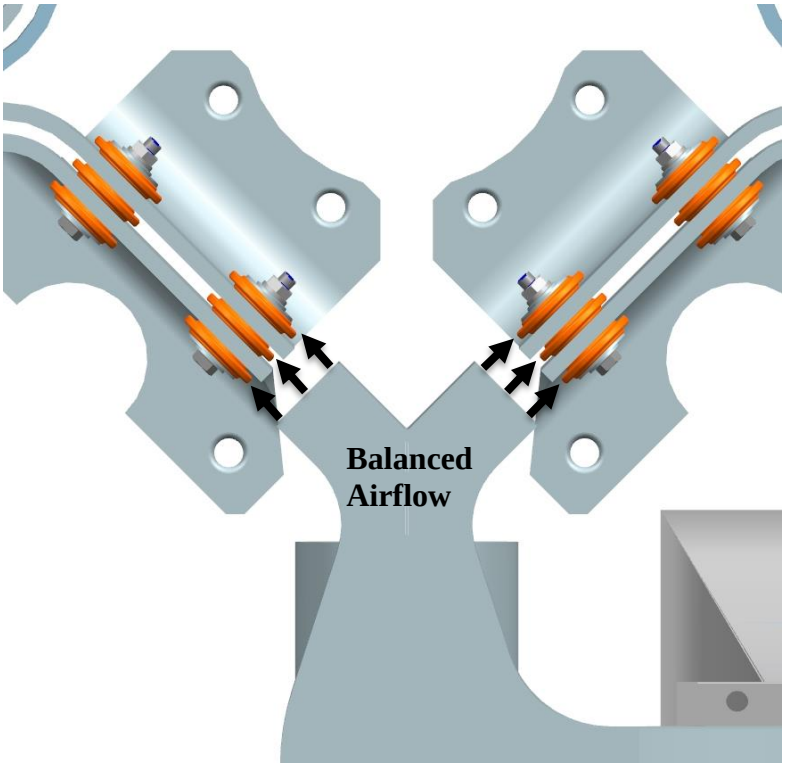

Figure 5.1.5 Revised outlet duct airflow.

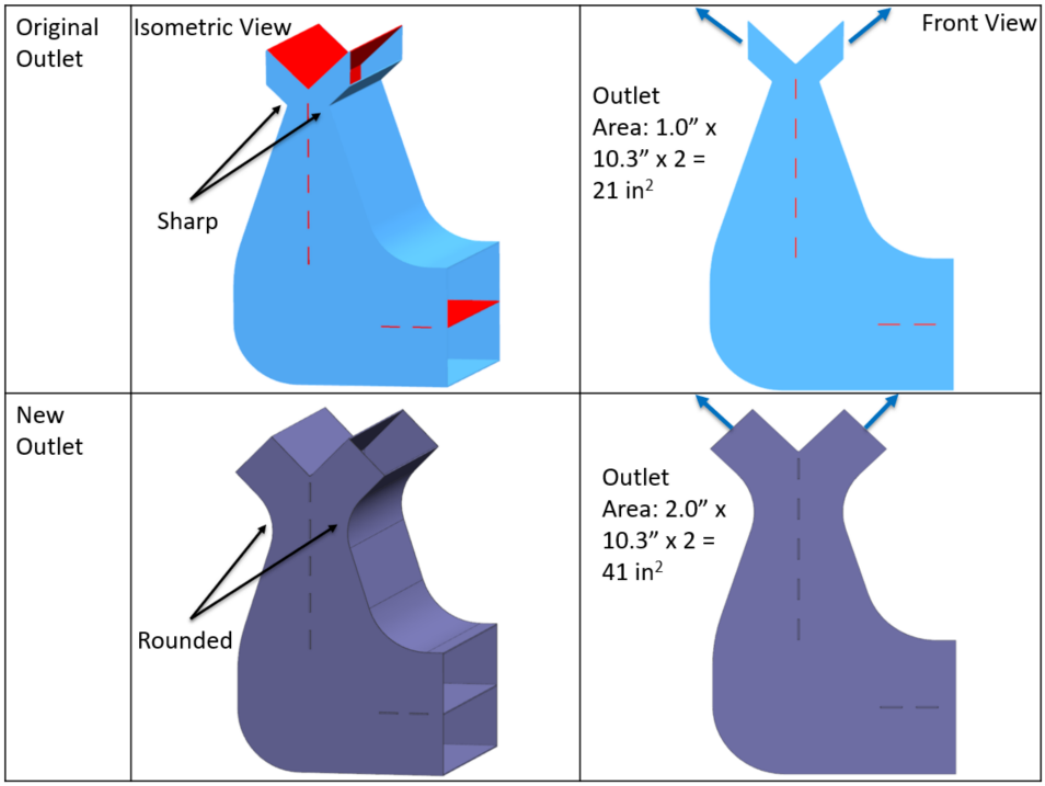

Figure 5.1.6 Outlet duct comparison.

2. Specifications

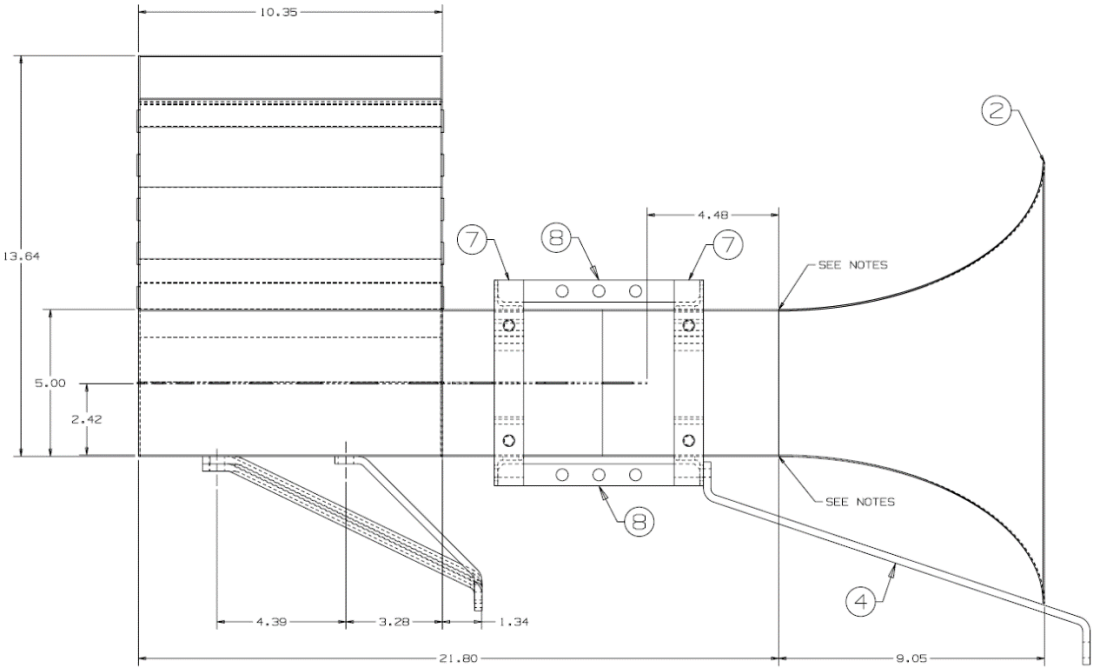

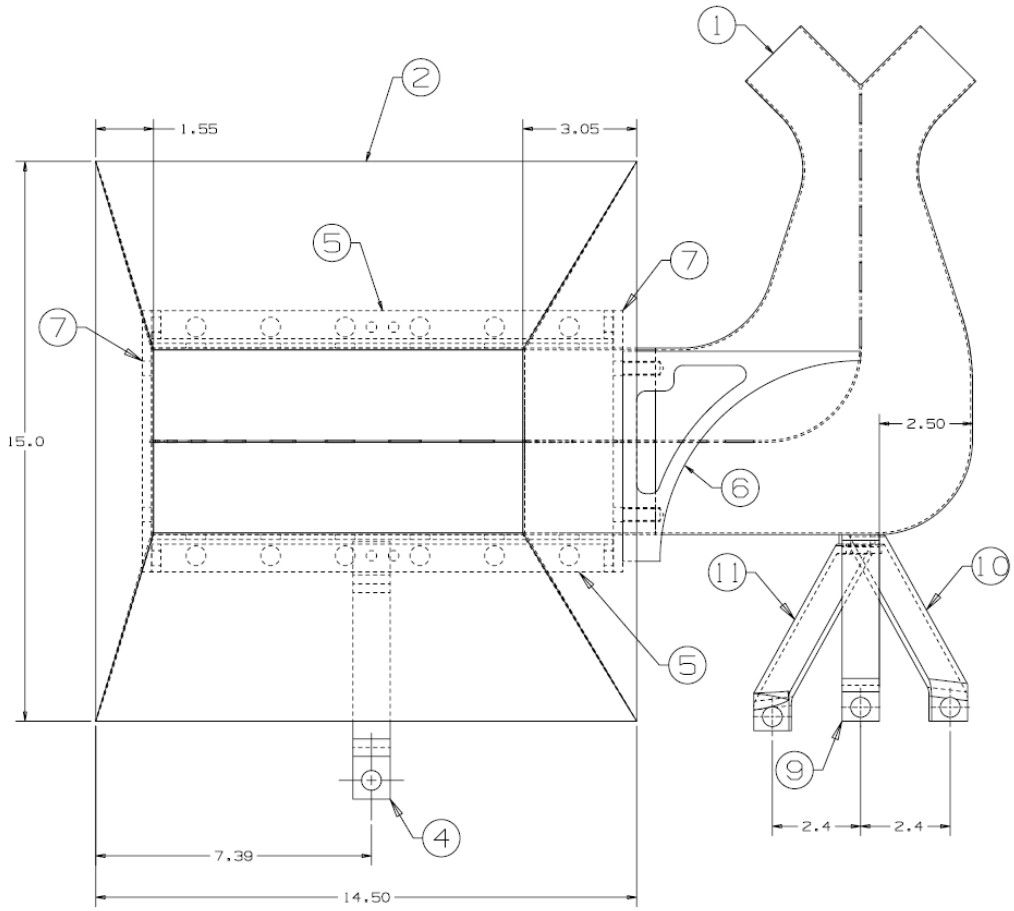

Figures 5.2.1 & 5.2.2. Upgraded diverter specifications.

VI. Supplemental T-Block Diverter

1. Initial Concept

The project anticipated an additional need to provide ducted air flow to the upper end of the stripline, as the upper flags and top end stripline block connection see little to no cooling gain with the original or even revised diverter. This flow would be provided through the use of a separate flow circuit, on the order of 600-1000 CFM, that is taken out of the main supply “pantleg” in the target hall (post cooling & dehumidification), run through an additional cooling coil if warranted, and down through the battlement penetration where it can mate to a cooling channel duct.

Initially, the upper stripline solution consisted of a ducted stripline shield block which contained the dedicated air pressure circuit to solve the operating temperature problem. Conceptually, the top of the stripline block lent itself to modification and sealing methods between stripline layers was proven in the target hall through the use of a Santoprene gasket. It became apparent however that although the stripline shield block main channel would indeed support air flow to keep the structure cool, that airflow would not be able to provide any effective cooling for the hottest regions near the conductor mounts.

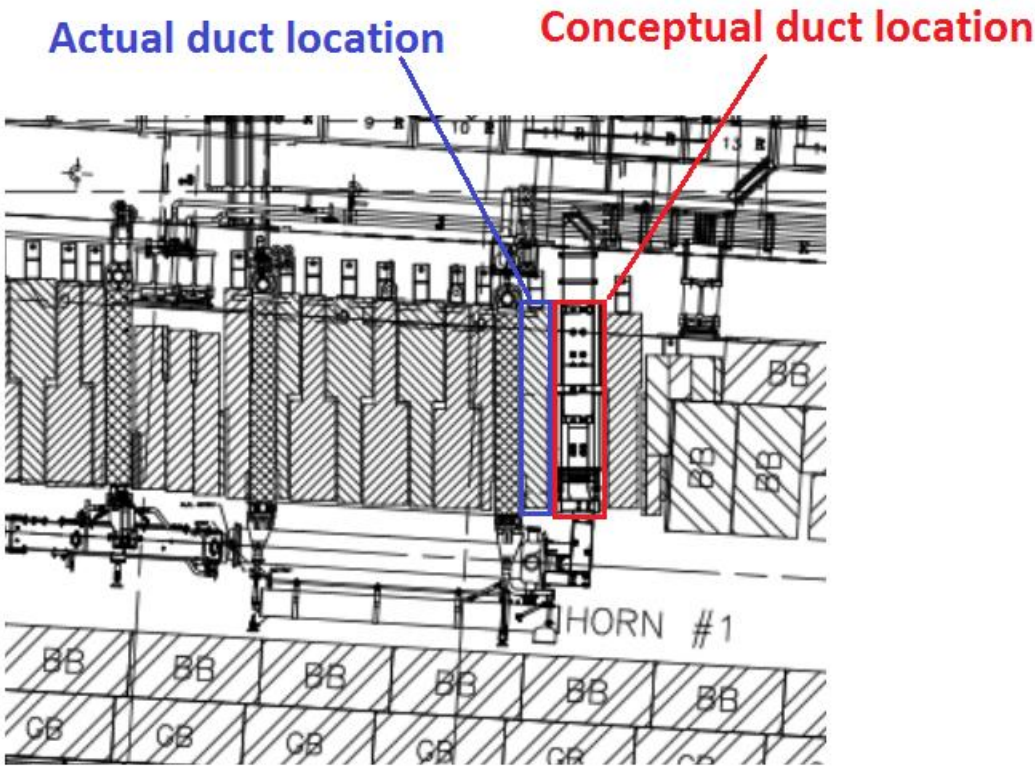

Figure 6.1.1 Conceptual air duct location vs. actual design proposed.

This concept (shown in RED above) was replaced with the idea of a dedicated cooling channel, routed through an adjacent shield block (shown in BLUE above). This solution has several benefits:

1. It requires a one-time replacement of a shield block for the remaining life of the experiment.
2. The existing operational stripline block, as well as all subsequent spares, would not need retrofitting with the duct system.
3. Running the air duct through a separate block eliminates an additional step for disconnecting a stripline block in what is typically the most activated area of the chase where technicians must work.
4. A dedicated adjacent cooling block can have a custom fit diverter suited to the application and geometry of the horn stripline. It does not rely on existing limitations at the bottom of a horn stripline block.

2. Pursued Design

The final solution of a dedicated cooling T-block, with an internal air channel and lower diverter pointed at the top end of the Horn 1 stripline is shown in figure 6.2.1. The T-block chosen was the single block located between the D.S. module end wall and the stripline shield block, which has direct access to the area in question, as well as enough space underneath to provide flexibility with duct design.

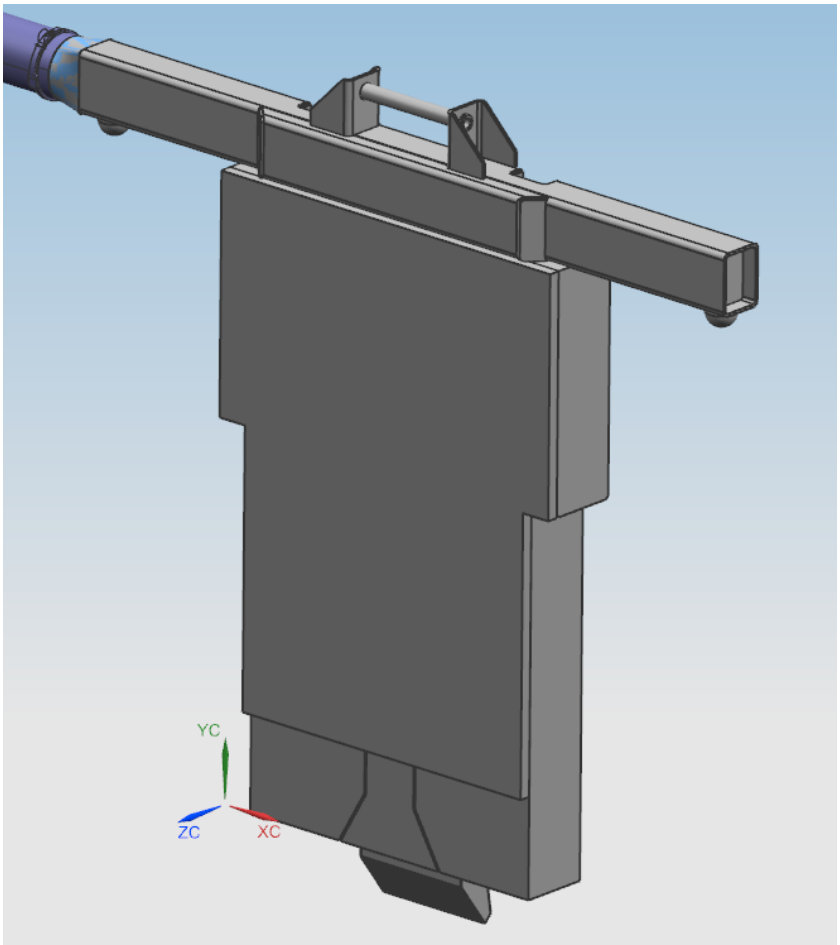

Figure 6.2.1 Proposed air diverter T-block.

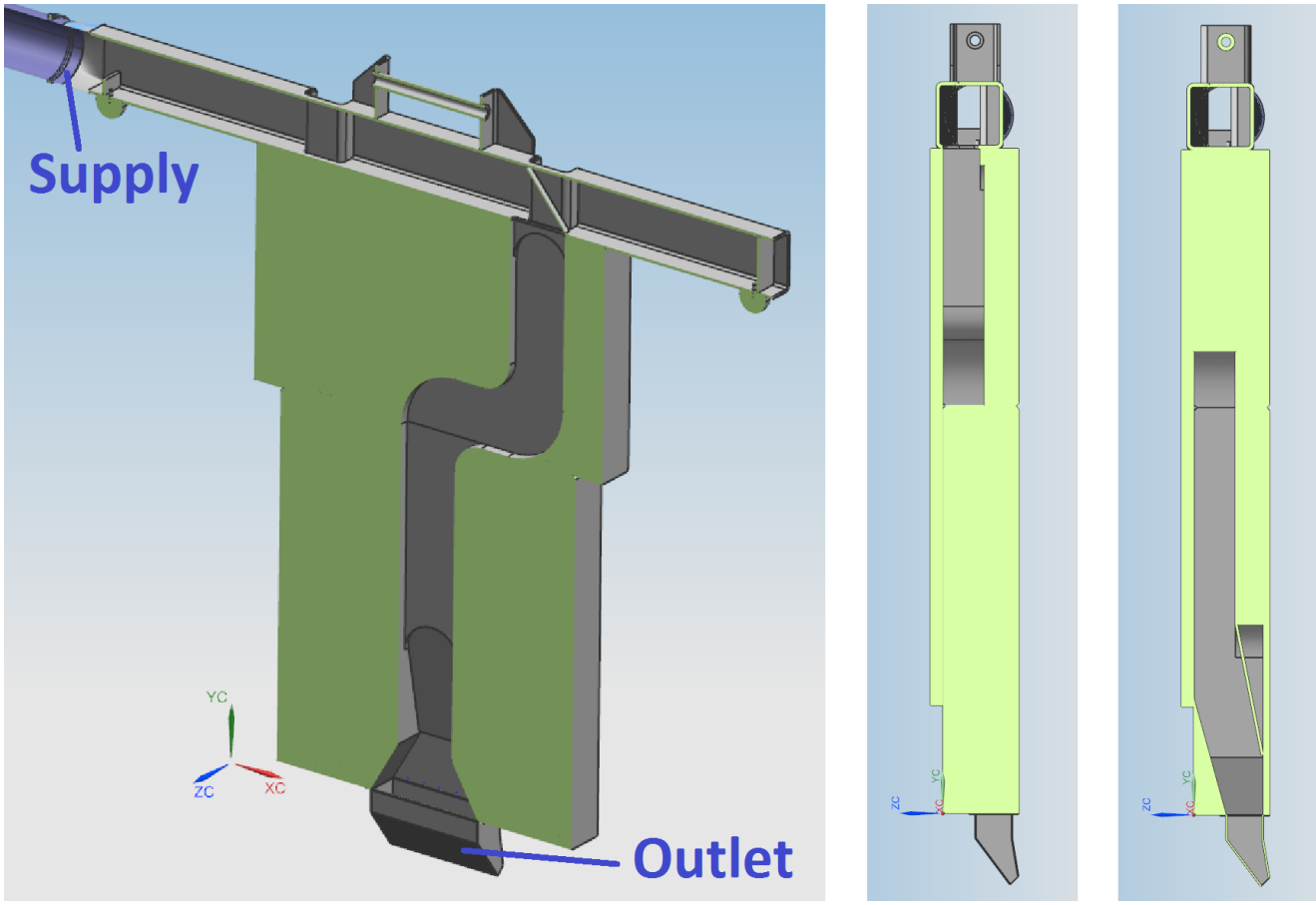

Figure 6.2.2 Cross-section view of proposed air diverter T-block.

Early pressure testing data and subsequent experimental runs with a forced flow main stripline diverter confirmed the hypothesis that the upper flag layers specifically, were lacking in sufficient heat transfer. This was most noticeable on the outer upper layers, as they are essentially unaffected by the existing ductwork, and even more susceptible to high temperature operation due to the blocked airflow from the top of the horn due to module mounting connections. Studies showed that although there was sufficient air mixing at the lower diverter with the main chase air flow, the mixing occurred further D.S. and somewhat lower than ideal with regards to the upper flags. Therefore, the dedicated air diverter T-block was to primarily focus on cooling the upper flags & stripline layers.

3. Diverter Angle Iterations

Test 1: 90 Degree Duct Outlet

The initial test utilized a duct outlet that provided air at a ~90 degree angle measured relative to the vertical supply direction (outlet is parallel with the beamline). This initial geometry assumed that the angled duct-work prior to the outlet would more so favor air flow at a downward angle as opposed to truly parallel with the beam. In testing, there indeed was an immediate and dramatic increase in measured cooling coefficient for the top flags. To try and visually quantify this, smoke tracing was attempted by feeding the smoke supply through the fan inlets, however the 600CFM flow rate of air used in testing was sufficiently high to dilute the produced smoke screen to the point of uselessness for

eddy current / flow direction tracking. Nonetheless, results were clear that the initial angle had a dramatic impact. One concern presented however was the inability to gauge what fraction of air flow was bypassing the stripline completely due to the parallel angle. Additional testing was warranted to try and subjectively gauge the losses, with the guide being measured convection coefficients.

Figure 6.3.1 90 degree upper diverter outlet.

Test 2: 0 Degree Duct Outlet

The second test performed at 0 degrees assumed that a large portion of the 90 degree supply duct air was completely missing the upper flags and getting swept up in the main chase air flow. The 0 degree duct was an attempt at gauging sensitivity of the cooling coefficients as they related to duct angle, as the 0 – 90 sweep essentially provided the two extreme air supply angles at the ends of the available range.

Test 3: 45 Degree Duct Outlet

The third test was an attempt at a close to ideal flow condition, as it was predicated on the idea that air losses relative to the main stream were minimalized, whilst trying to earn back some of the losses experienced when switching to the 0 degree duct outlet angle. Data shows that this outlet angle yields the highest recorded heat transfer coefficients for the upper flags, and so is experimentally shown to be near ideal relative to the other two angles tested. It is likely that small variations of the 45 degree duct outlet, possibly in the ranges of 20-70 degrees would be more beneficial, but subsequent testing time was limited, and the solution presented yields acceptable results for 1MW operation of the revised stripline design.

Figure 6.3.2 45 degree upper diverter outlet.

4. Final Model

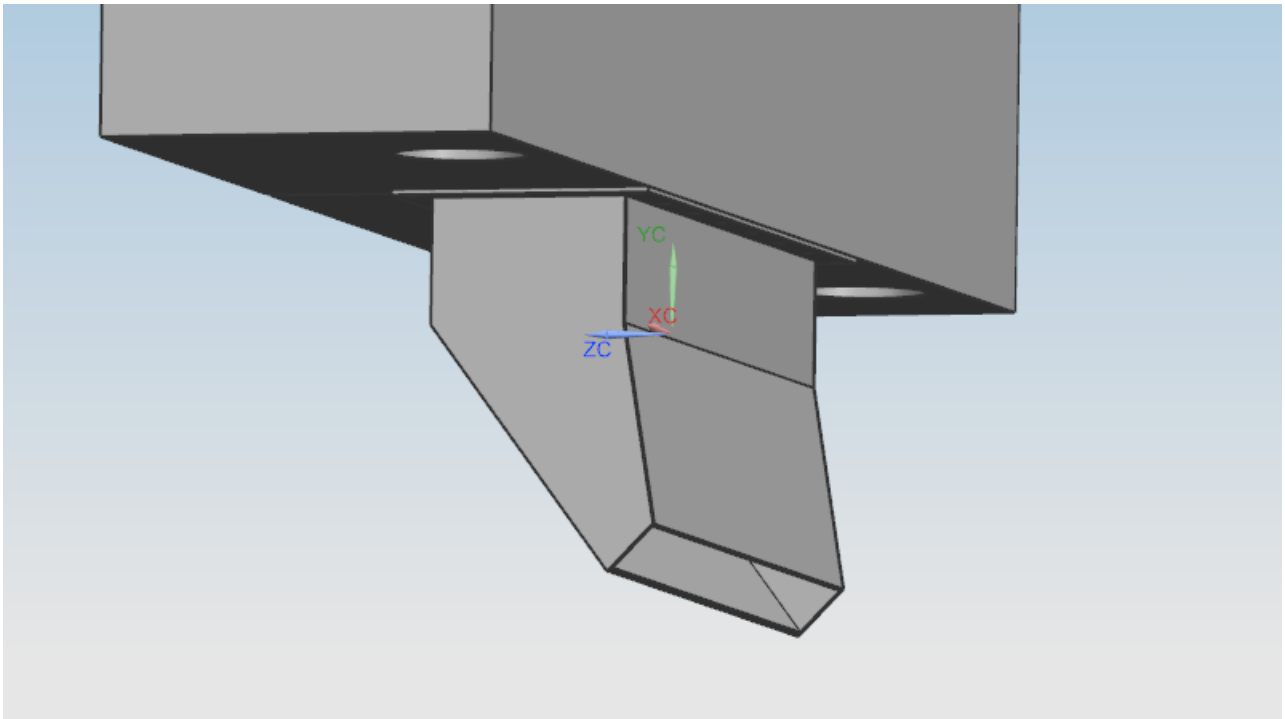

Figure 6.4.1 Final diverter model as mounted to ducted T-block.

VII. Experimental Convection Coefficient Data

1. Test Setup

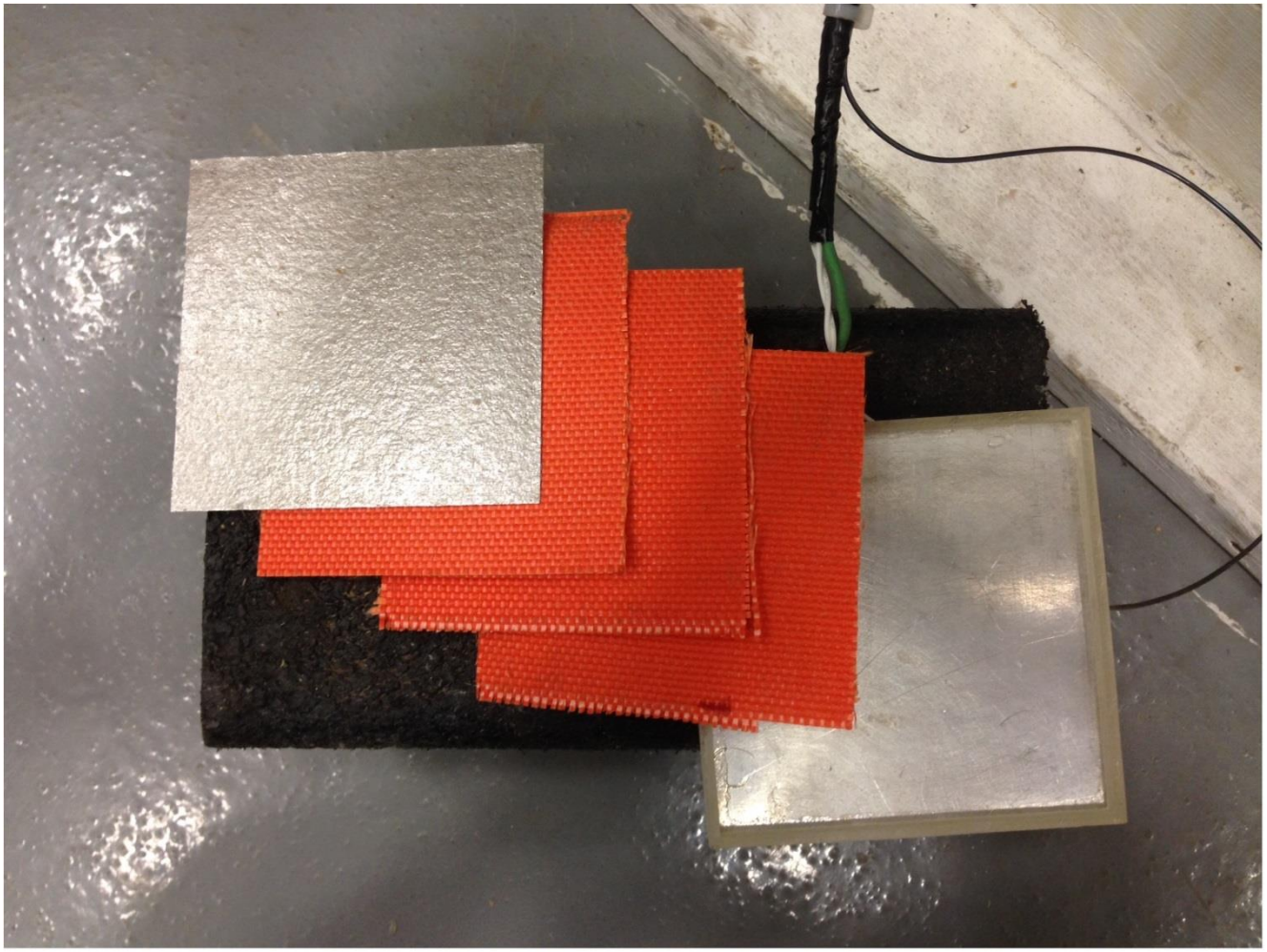

Figure 7.1.1 Thermal isolation layers (3 fiberglass matts + .010” mica sheet).

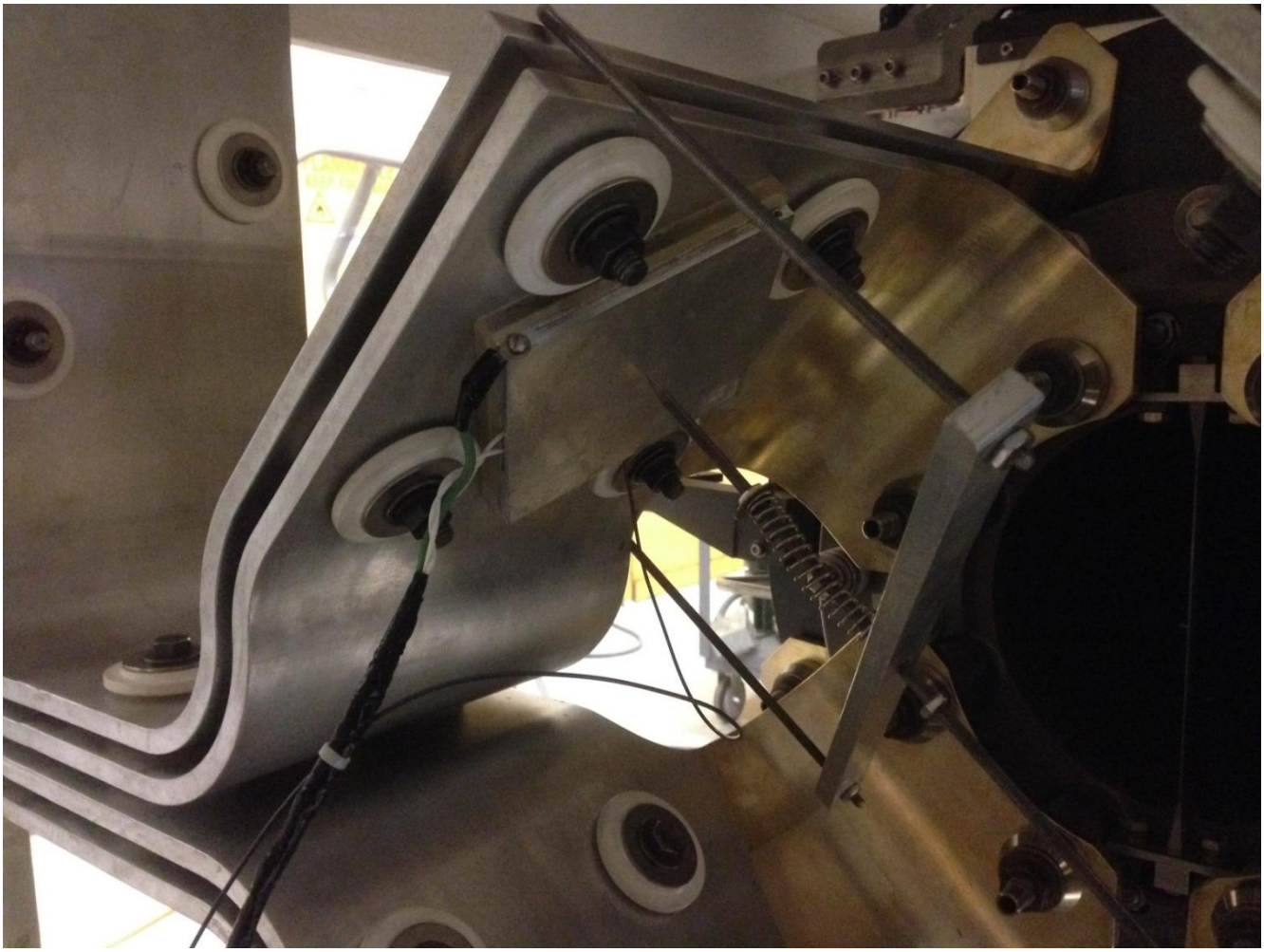

Figure 7.1.2 Heated coupon placement on stripline.

2. Data

Test # / Flag	BRLFO			BLLFO			BRLFI			BLLFI		
	Eq. Temp	Power	h	Eq. Temp	Power	h	Eq. Temp	Power	h	Eq. Temp	Power	h
T3	N/A	N/A	N/A	N/A	N/A	N/A	N/A	N/A	N/A	N/A	N/A	N/A
T4	N/A	N/A	N/A	N/A	N/A	N/A	N/A	N/A	N/A	N/A	N/A	N/A
T5	N/A	N/A	N/A	N/A	N/A	N/A	241.45	80	73.18	242.63	80	72.67
T6	250	72.32	62.97	250	80	69.66	237.23	80	75.05	237	80	75.15
T7	250	80	69.59	250	73.6	64.09	231.19	80	77.9	235.8	80	75.7
T8	250	80	69.6	250	75.4	65.66	236.8	80	75.24	218.6	80	84.58

Table 7.2.1 Test runs 3-8 for beam right and left lower inner and outer flags.

Test # / Flag	BRUFO			BLUFO			BRUFI			BLUFI		
	Eq. Temp	Power	h	Eq. Temp	Power	h	Eq. Temp	Power	h	Eq. Temp	Power	h
T3	174.27	80	121.25	195.5	80	100.4	196.87	80	99.31	207.71	80	91.37
T4	211.23	80	89.06	209.54	80	90.15	209.86	80	89.95	212.97	80	87.96
T5	213.89	80	87.39	211.84	80	88.67	N/A	N/A	N/A	N/A	N/A	N/A
T6	212.62	80	88.18	210.4	80	89.59	250	67.58	58.85	250	64.5	56.16
T7	237.96	80	74.72	234.32	80	76.39	250	68.2	59.32	250	68.2	59.39
T8	172.26	80	123.67	175.33	80	120	250	66	57.47	249.65	80	69.8

Table 7.2.2 Test runs 3-8 for beam right and left upper inner and outer flags.

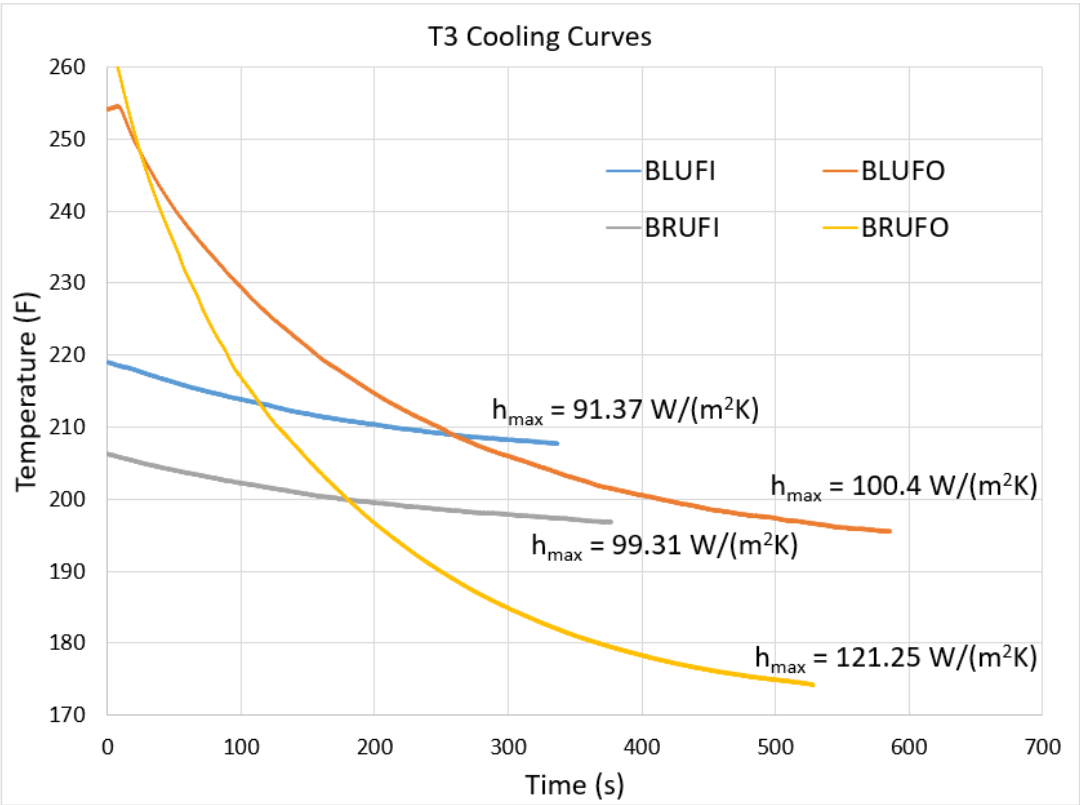

Figure 7.2.1 T3 Test Data.

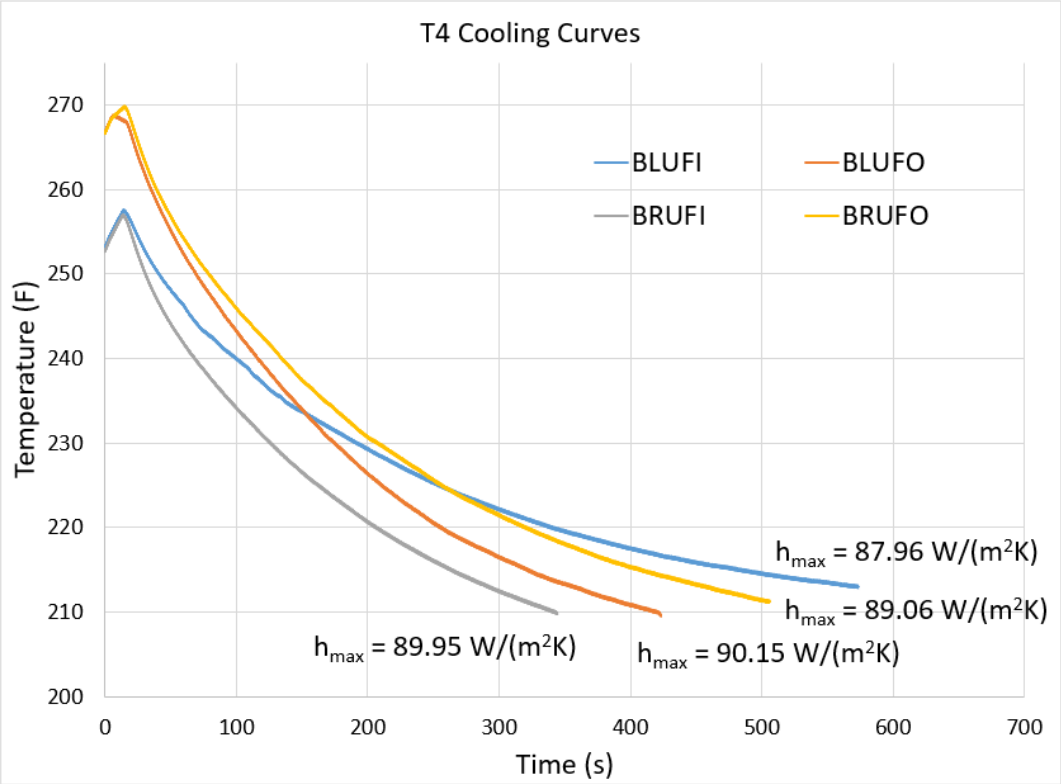

Figure 7.2.2 T4 Test Data.

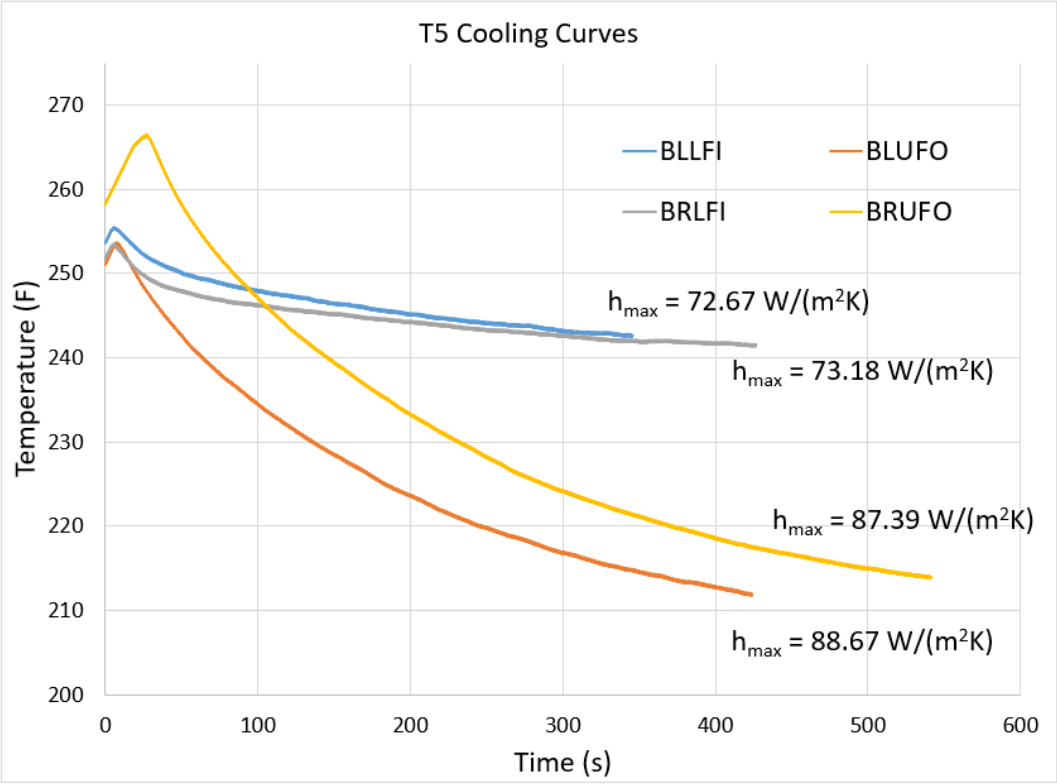

Figure 7.2.3 T5 Test Data.

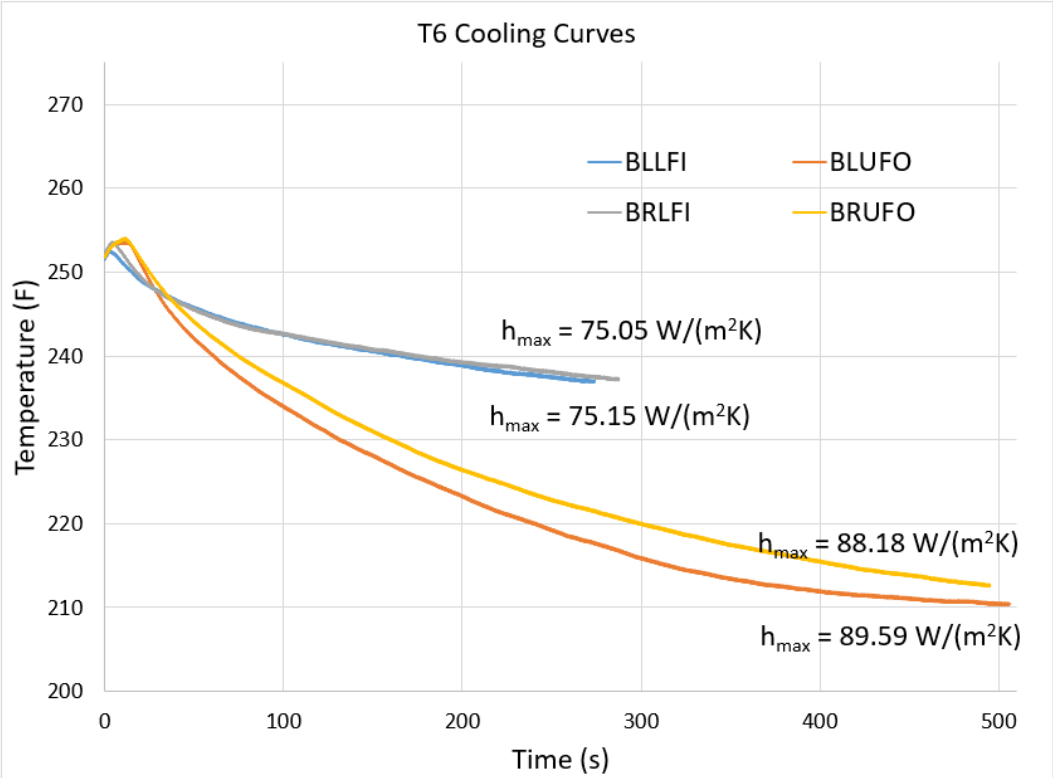

Figure 7.2.4 T6 Test Data.

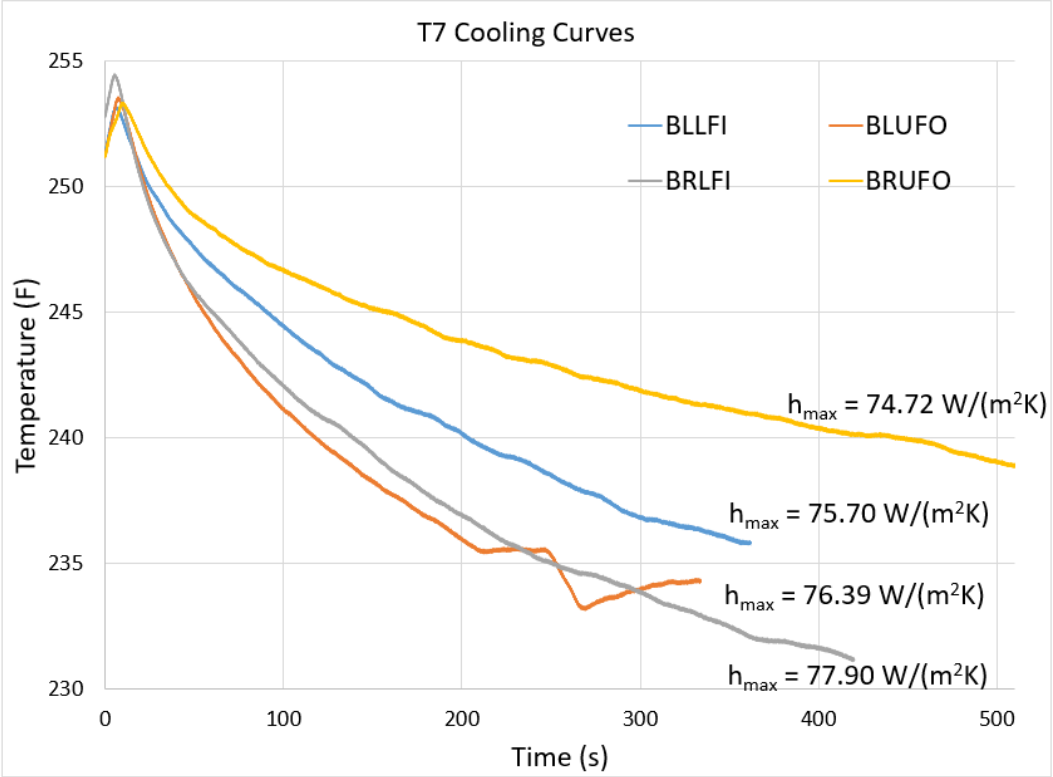

Figure 7.2.5 T7 Test Data.

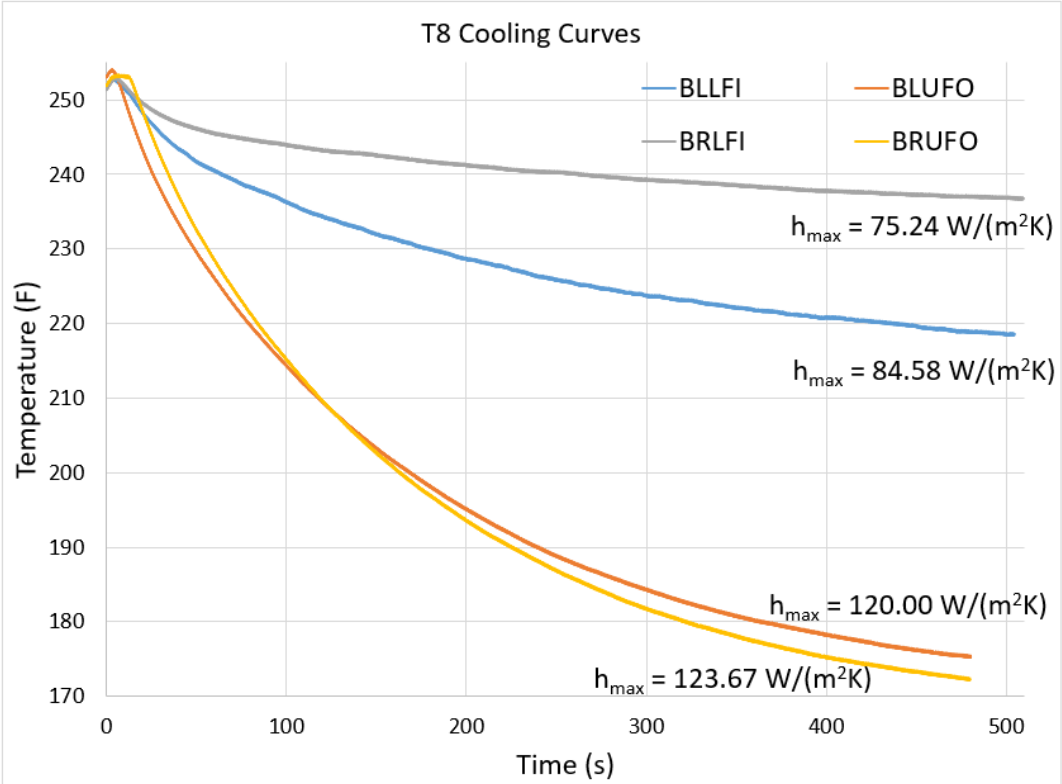

Figure 7.2.6 T8 Test Data.

3. Inner Stripline Testing

Because the inner strip line pieces are so close together, shown in figure 7.1.2, a novel way for measuring the convection coefficient in between the plates was needed. In the past, the air between the plates was assumed to be stagnant with a convection coefficient of 5 W/(m^{2}K). To experimentally determine a more realistic value, a test bed was created simulating the plate geometry. Shown in figure 7.3.1, the test bed features a 3-shelf design with 2 pieces of 4.25in x 4.25in x 0.375in strip line on the top and bottom shelves, and the heating coupon on the middle shelf. Similar to the previous cooling curve tests, a thermocouple was placed inside the middle coupon and it was heated to a temperature of approximately 212°F.

The top diverter as well as the main channel air flow were then turned on and the coupon was allowed to cool to a steady state temperature. In addition, a thermocouple was placed on a strip line coupon adjacent to the heated coupon in order to observe the heated coupon's radiative effects on surrounding plates. The test was conducted with the test bed mounted on the Beam Left Upper Flag and Beam Left Lower Flag locations and the data is presented in figures 7.3.3 and 7.3.4 respectively. The experimentally determined convection coefficient was averaged between the two tests, de-rated, and the same value was assumed for the Beam Right location.

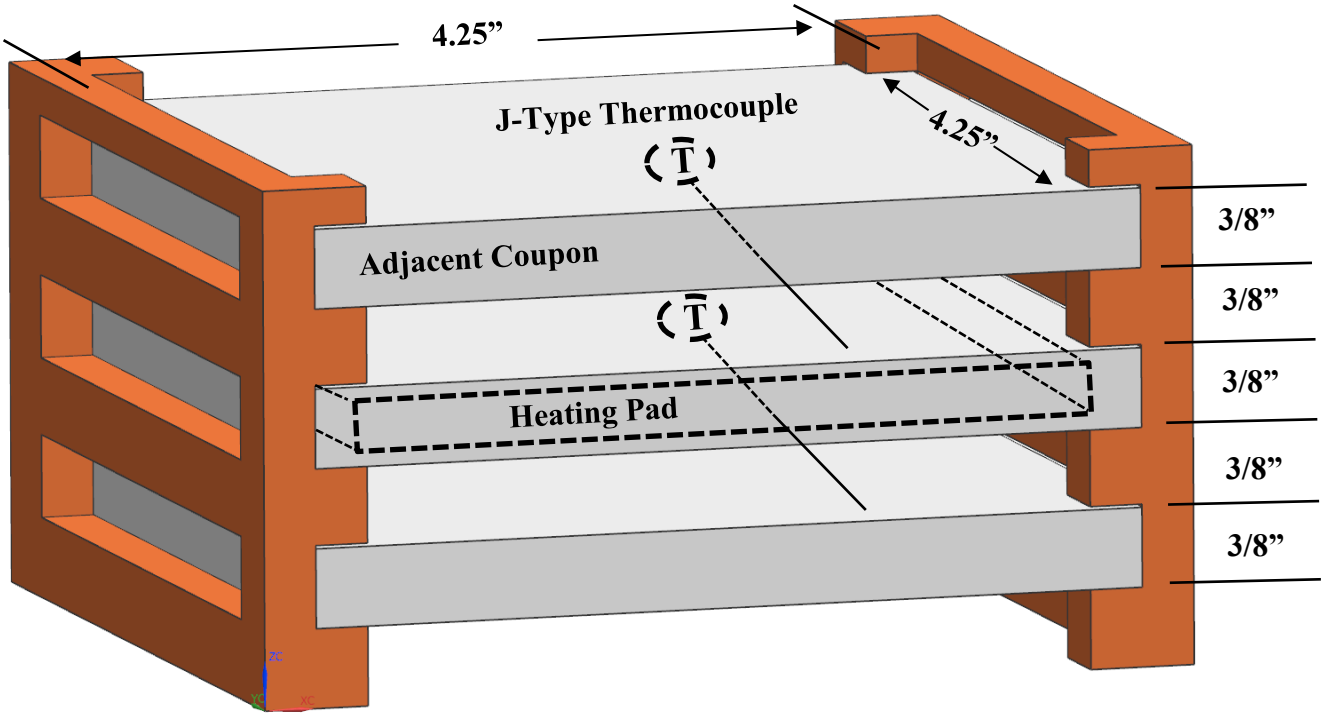

Figure 7.3.1 Inner layer test setup.

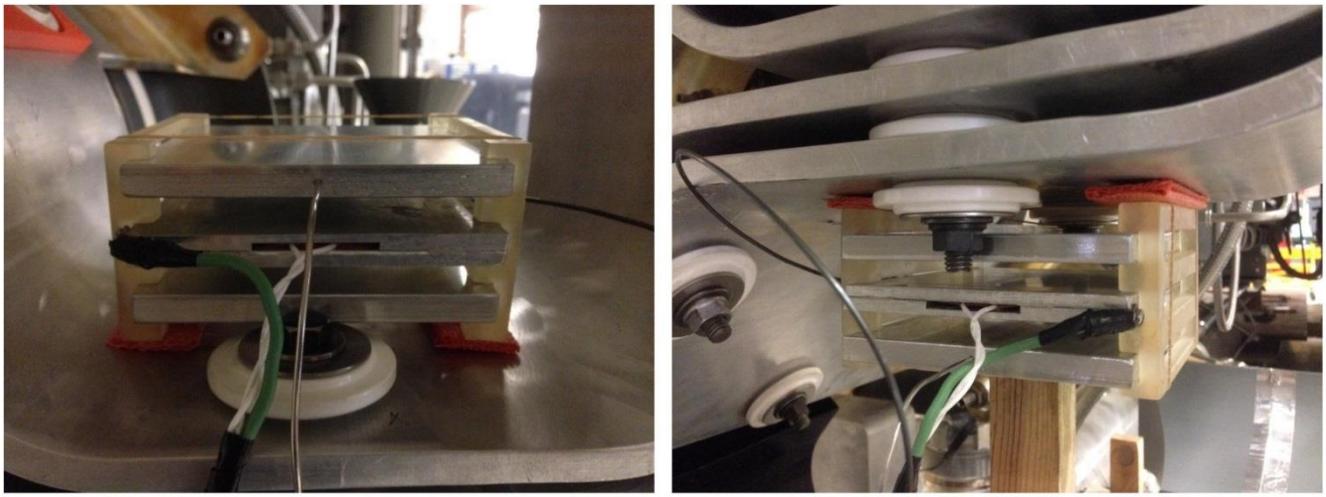

Figure 7.3.2 Inner layer experimental test.

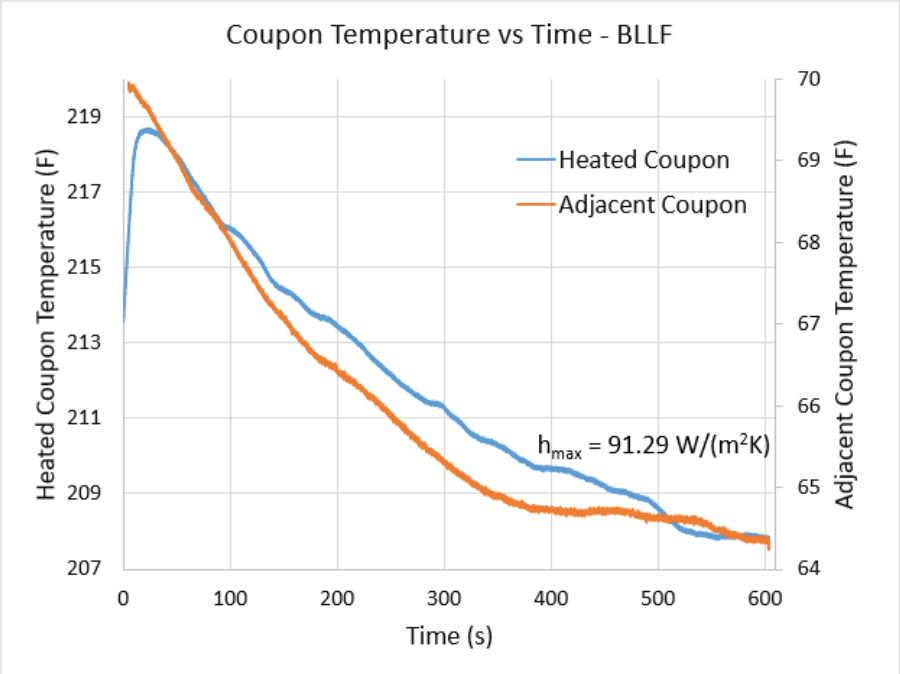

Figure 7.3.3 T3 Test Data.

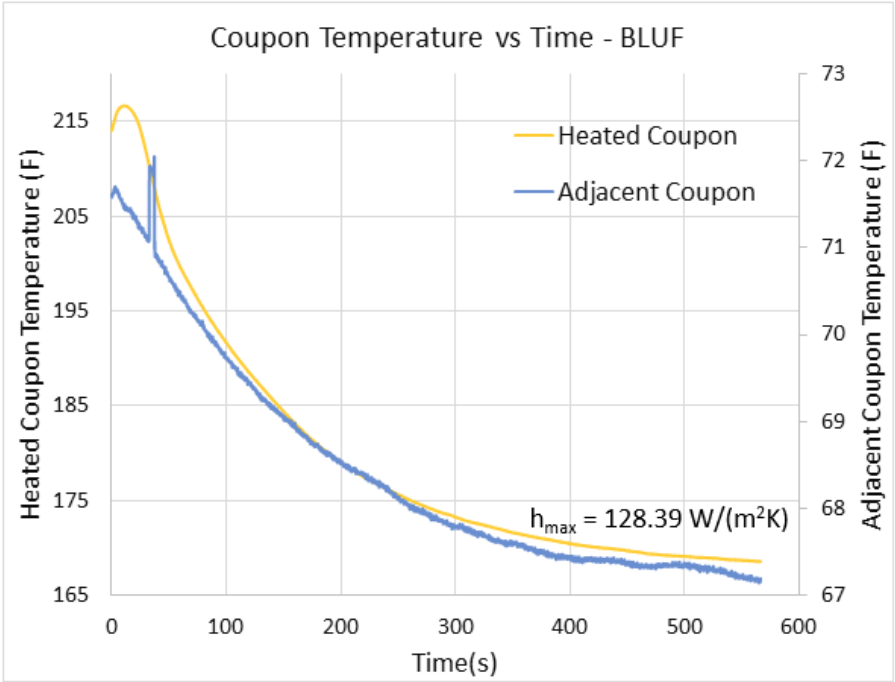

Figure 7.3.4 T3 Test Data.

VIII. Updated 1MW Stripline Analysis

1. Steady State Temperature

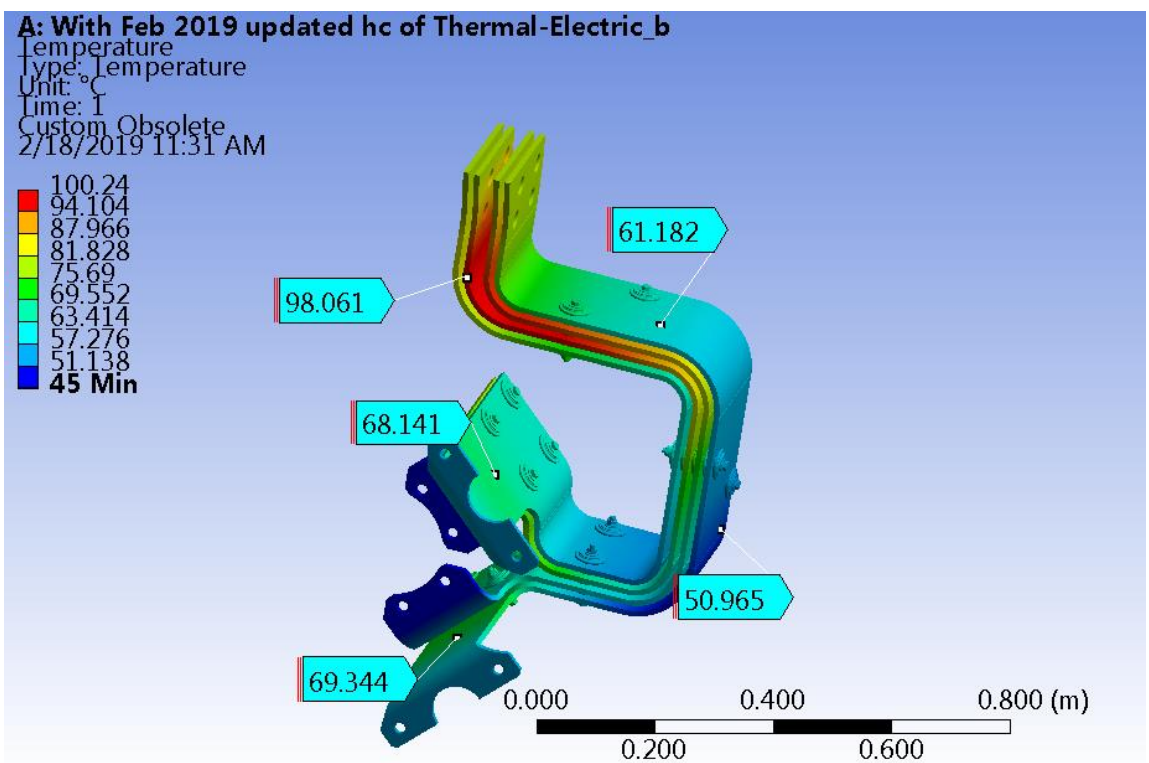

Figure 8.1.1 Steady state temperature of aluminum stripline layers.

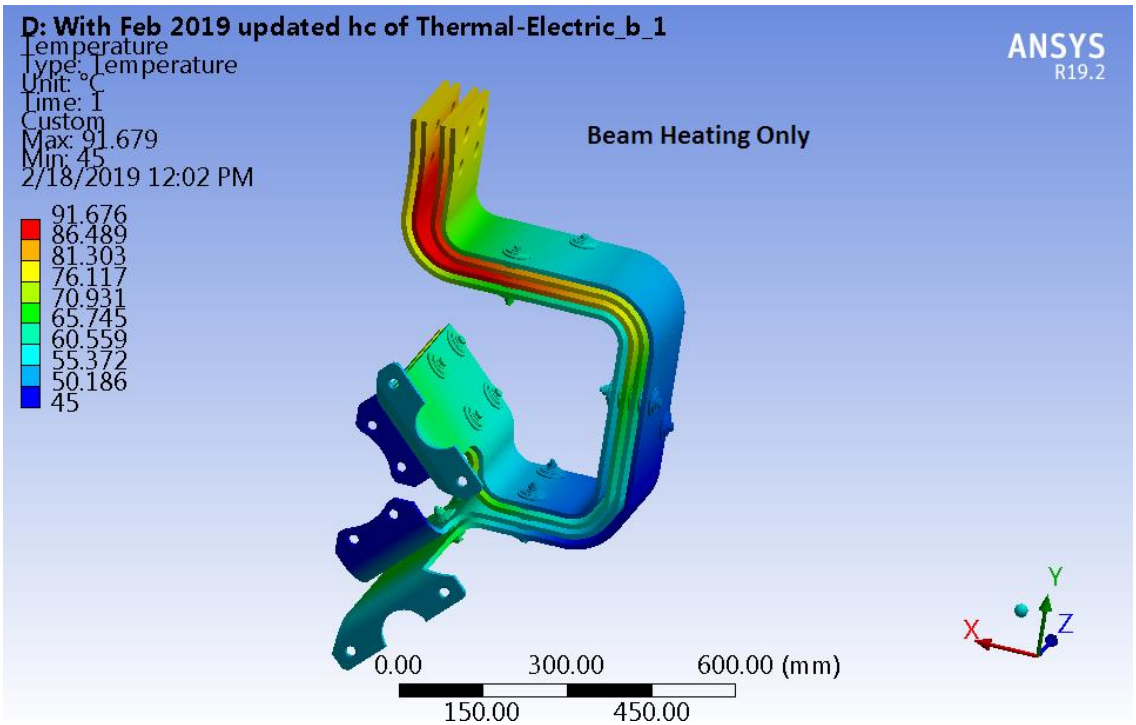

Figure 8.1.2 Steady state temperature contribution of beam heating only.

2. Transient temperature

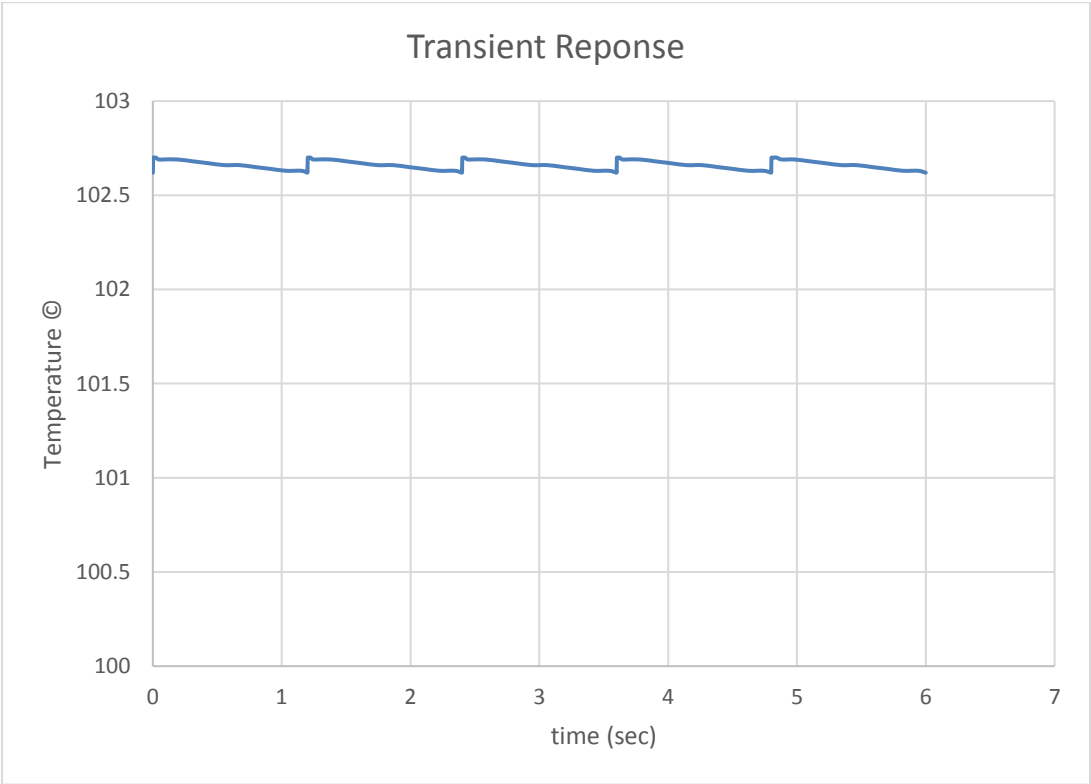

Figure 8.2.1 Transient thermal response of stripline assembly.

3. Total Deformation

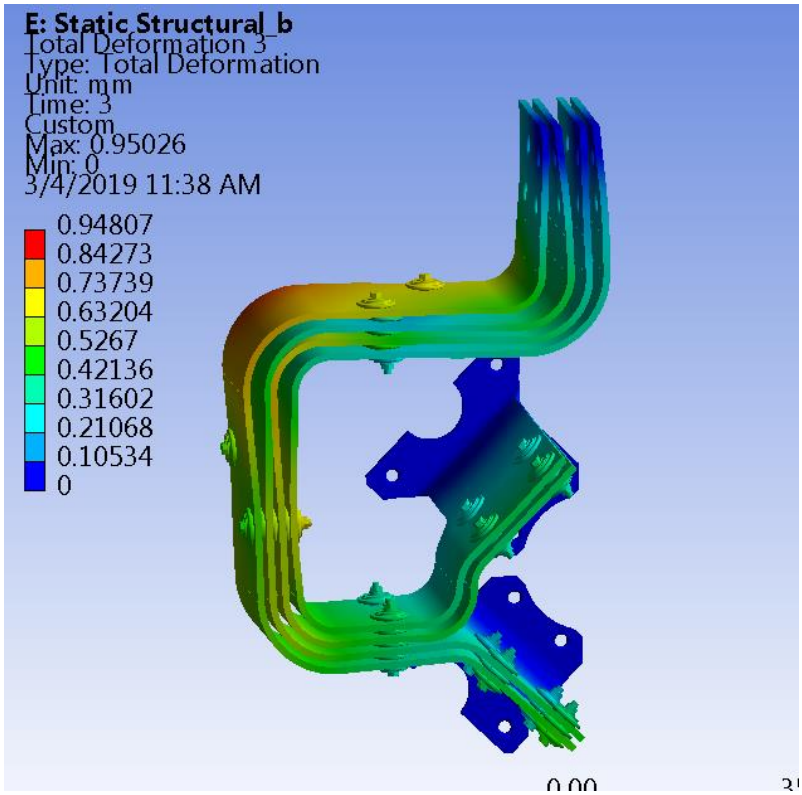

Figure 8.3.1 Total deformation of stripline assembly.

4. Transient Stress

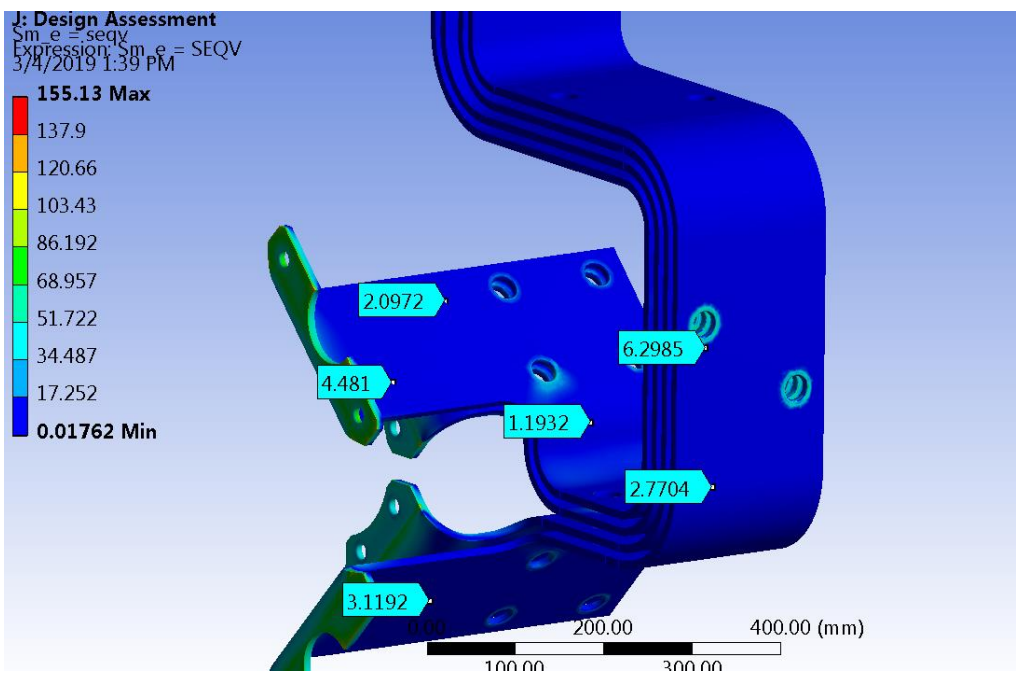

Figure 8.4.1 Transient stress of stripline assembly (mean stress).

IX. Conclusion

Efforts to increase the convection cooling coefficient on the 1MW NuMI / NOvA Horn 1 stripline structure were successful. The dual approach of an improved lower air diverter coupled with the additional T-block upper diverter effectively doubled or tripled the known convection coefficients from prior testing. These new values, when applied to the axisymmetric finite element model, yield acceptable maximum temperature results near ~100C, which is the maximum acceptable aluminum operating temperature for components in the NuMI beamline.

The stripline structural results also show acceptable stresses in the bulk material, with the exception of localized yielding at the bolt holes due to mesh size and / or stress concentrations. These stresses are thermally induced however, and therefore are a secondary or "relenting" stress, that will decrease with time after undergoing initial yielding when first reaching maximum operating temperature. The predominate stress is caused by the bolt preload, which is a purposeful artifact of efforts to keep the structure contained. Final safety factor results for the bulk stripline structure can be seen in table 10.1 below.

SF (min)	Stripline Bulk Structure	Bolt Hole	Connection to Horn Flange
Al 6101-T6	SF > 5	SF = 1.64 (based on the peak number)	N/A
Al 6013-T6	SF > 4	SF = 2.5 (based on the peak number)	SF = 2 (based on the peak number)